Modeling the impacts of climate change on streamflow of the Nicolet River as affected by snowmelt using ArcSWAT

Fei Tang
Department of Bioresource Engineering
McGill University, Montreal
Quebec, Canada

A thesis submitted to McGill University in partial fulfilment of the requirements of the degree of Master of Science

Table of Contents

Abstract

Responsible for spring peak flows in southern Quebec's Nicolet River watershed, snowmelt runoff may, upon a rapid rise in temperature, reach flood stage. The impacts of climate change on the basin's hydrology were assessed by comparing Soil and Water Assessment Tool (ArcSWAT) simulations of Nicolet River streamflow drawing on historic and projected climatic data. Calibrated with streamflow data measured between 1986 and 1990, and validated with 1991-2000 data, ArcSWAT proved reliable in simulating streamflow: the Nash-Sutcliffe efficiency exceeded 0.50, while the percent bias and root mean squared error-observations standard deviation ratio remained below ±15% and 0.70, respectively, across both model development phases. Drawing on climate projection inputs, the ArcSWAT model shed light on the potential impacts of climate change: rising precipitation would directly alter surface runoff, while a concomitant rise in temperature would affect evapotranspiration, snowfall, and winter snowmelt.

A comparison of simulated Nicolet River streamflow characteristics under current (1986-2000) and eleven projected future climate datasets (2053-2067) obtained by embedding the Regional Climate Model (RCM) into the Global Climate Model (GCM), showed a consensus that average temperature would rise by 2.6℃ and precipitation by 21%, with the increase being particularly significant in winter. On average, snowfall was projected to decrease by 6%. The snowmelt was projected to decrease in total volume, but be more concentrated in late winter and earlier spring. General increases were expected in mean annual, summer, autumn and winter streamflow, but spring flow was expected to decrease. Averaged across all scenarios, peak flows were predicted to increase by 13%, and occur earlier. A study separating the effects of temperature and precipitation under future climatic conditions showed that the increases in the magnitude of peak flow were

mainly attributable to the increased precipitation, whereas timing of the peak was mostly influenced by the increase in temperature.

Résumé

Responsable du débit de pointe printanier dans le bassin versant de la rivière Nicolet situé dans le sud du Québec, le ruissellement provenant de la fonte des neiges peut engendrer une inondation si la température augmente rapidement dans un court délai. Ayant entrepris dans cette étude de modéliser le débit de la rivière Nicolet, Les effets du changement climatique sur le comportement hydrologique de ce bassin versant furent étudiés en comparant les caractéristiques des débits historiques à ceux modélisés pour l'avenir par le Soil and Water Assessment Tool (ArcSWAT) selon des données climatiques provenant de divers scénarios de l'évolution du climat. Étalonné et validé selon les débits de la rivière Nicolet mesurés entre 1986 et 1990 et entre 1991 et 2000, respectivement, le modèle ArcSWAT s'avéra un outil fiable pour la modélisation du débit [biais (%) en deçà de 15%, coefficient d'efficacité Nash-Sutcliffe > 0.50 et le rapport erreur quadratique moyenne à l'écart type des observations, RSR < 0.70] à la fois pour les phases d'étalonnage et de validation. Mû par les données climatiques d'entrée, le modèle ArcSWAT démontra sa capacité de simuler la réaction du bassin versant aux changements climatiques: une hausse des précipitations influenceraient directement le ruissellement en surface, tandis qu'un changement simultané de la température influencerait aussi l'évapotranspiration, l'abondance des chutes de neige, et les fontes de neige hivernales.

Une comparaison des caractéristiques du présent débit (1986-2000) à ceux advenant d'onze jeux de données projetées pour 2053-2067 provenant d'un modèle climatique régional (MRC) intégré à l'intérieur d'un modèle climatique global (GCM), montre un consensus que la température moyenne augmentera de 2.6°C et la précipitation de 21%), particulièrement en hiver. En moyenne, les chutes de neige devraient diminuer de 6%, le volume total de la fonte des neiges devrait diminuer, quoiqu'il augmentera en fin d'hiver et au début du printemps. En général, le débit estival,

automnal, hivernal et annuel moyen augmenteront, tandis que le débit printanier diminuera. Ayant moyenné tous les scénarios climatiques, l'on s'attend à une augmentation de 13% des débits de pointe, qui auront lieu plus tôt. Une étude discriminant entre les effets des changements projetés de la température et de la précipitation sur les débits de pointe, démontra que leur ampleur est plutôt liée aux augmentations en précipitation, et leur échéance aux augmentations de température.

Acknowledgements

I would like to express my sincere appreciation to my supervisor Dr. Zhiming Qi for his constant guidance, and his encouragement throughout my research. I am also grateful to my lab mates, Hongkai Qi, Qianjing Jiang, Che Liu, Changchi Xian, Rasika Burghate, Debasis Sahukhan, Mariam Sorour and Mahsa, who made my stay and study in Canada more enjoyable.

I would like to thank all my friends, especially Lei Tian, Yakun Zhang, Jianhui Huang, and Sirui Li. You make my life colourful and wonderful. Finally, I would like to thank my mother and father for their unfailing support and continuous encouragement throughout my years of study and through the process of research and writing this thesis.

List of Tables

List of Figures

List of Abbreviations

b_{mlt}: melt factor for the day

b_{mlt6}: melt factor for June 21

b_{mlt12}: melt factor for December 21

cov_1 and cov_2: coefficients determining curve shape

d_n: is the n^{th} day of a year.

h_{wtbl}: water table height

k_{sat}: saturated hydrologic conductivity

slp: elevation per unit distance or slope

sno_{cov}: fraction of the HRU area covered by snow

t : time

t_{ov}: is the overland flow time of concentration

w_{seep_i}: quantity of water entering the vadose zone from the soil profile on day i

ALPHA BF: baseflow recession factor

ArcSWAT: ArcGIS-ArcView extension and graphical user input interface for SWAT

CH_N(1): Manning‘s “n” value for tributary channels

CN: SCS curve number

CRCM4: Canadian Regional Climate Model

DEM: digital elevation model

DDF: Degree-day factor

E_{sub_i}: quantity of sublimation on a given day *i*

EPC: Emergency Preparedness Canada

EPCO: plant uptake compensation factor

ERR_{wb}

ESCO: soil evaporation compensation factor

$E_{soil,y}$: evaporative demand for soil layer ly

$E_{soil,zl}$: evaporative demand at the lower boundary of the soil layer

$E_{soil,zu}$: evaporative demand at the upper boundary of the soil layer.

ET_{a_i}: quantity of evapotranspiration on day *i*

ET_a: actual evapotranspiration

ET_p: potential evapotranspiration

FRST: Forest-Mixed landuse

GW_DELAY: groundwater delay time

GW_REVAP: groundwater revap coefficient

GW_Q: groundwater contribution to streamflow

GWQMN: groundwater threshold depth

HAY: hay land use

HRU: hydrologic response unit

I_a: initial abstractions from rainfall, including surface storage, interception and infiltration prior to runoff

IPCC: International Panel on Climate Change

LAI: leaf area index

LATQ: lateral flow contribution to streamflow

L_{hill}: hillslope length

L_{slp} is the average slope length

M: quantity of ice and/or snow melt (or per unit time)

M_f : melt factor (mm $°C^{-1}$ h^{-1})

NARCCAP: North American Regional Climate Change Assessment Program

NSE: Nash-Sutcliffe coefficient

OV_n: Manning's roughness coefficient

PBIAS: Percent bias

PCBs: polychlorinated biphenyls

PRECIP: total precipitation

PRMS: USGS Precipitation-Runoff Modeling System

Q_e: latent heat flux (evaporation, sublimation, condensation) at the snow-air interface

Q_g: heat flux from the snow ground interface by conduction

Q_{gw_i}: quantity of return flow or groundwater flow into the main channel on day *i*

Q_h: convective or sensible heat flux from the air at the snow-air interface

Q_{lat}: lateral flow per day

Q_{ln}: net long-ware radiation flux at the snow-air interface

Q_m: energy flux available for melt

Q_p: flux of heat from rain,

Q_{sn}: net short-ware radiation flux absorbed by the snow

Q_{surf_i}: quantity of surface runoff on day *i*

RCPs: Representative Concentration Pathways

R_{day_i}: quantity of precipitation on day *i*

R_i : quantity of snowfall on a given day *i*

RMSE: Root Mean Squared Error

RSR: RMSE-observations standard deviation ratio

S: is the retention parameter

SFTMP: mean snowfall temperature

SLOPE: sub-basin slope

SLSoil: slope for lateral flow

SLSUBBSN: average sub-basin slope length

SMFMN: minimum snowmelt rate / melt factor for snow on December 21

SMFMX: maximum snowmelt rate/ melt factor for snow on June 21

SMTMP: snowmelt base temperature

SNO_{100}: threshold depth of snow at 100% coverage

SNO_i: snowpack water for a given day *i*

SNO_{mlt_i}: quantity of snow melt on a given day *i*

SNO50COV: 50% snow cover fraction

SNOCOVMX: 100% snow cover equivalent

SOL_AWC: available soil water content

SLOPE: slope of sub-basin

SLSOIL: slope for lateral flow

SMFMN: minimum snowmelt rate

SMFMX: maximum snowmelt rate

SMTMP: base snowmelt temperature

SN050COV: 50% snow coyer fraction

SNOCOVMX: 100% snow coyer equivalent

SOL_AWC: available soil water content

SURLAG: surface runoff lag coefficient

SURQ: surface runoff contribution to streamflow during time step

SWAT: The Soil and Water Assessment Tool

SWM: Stanford Watershed Model

$SW_{ly,xs}$: water stored in the saturated zone of the hillslope per hydrological unit

T_b: base temperature (usually 0°C)

T_i: index air temperature

T^+: sum of air temperatures over a given period

TLOSS: transmission losses from tributary channels

USDA: United States Department of Agriculture

USGS: United States Geological Service

USUWSM: Utah State University Watershed Simulation Model

WETN: Wetland-Non-Forested land use

WYLD: total water yield

α_{gw}: baseflow recession constant

Δt: a small period of time

$\Delta\theta$: change in soil water content

μ: is the specific yield of the shallow aquifer

θ_{fc}: soil moisture content at field capacity

θ_0: initial soil water content

θ_t: final soil water content (mm)

$\emptyset_d$: porosity of the soil layer at field capacity (θ_{fc})

Chapter 1 Introduction

1.1 Background

In Quebec, high flow events and spring floods are particularly affected by snowmelt, which accounts for up to 40% of annual streamflow (Coulibaly et al., 2000; Ferguson, 1999). During the period of 1900-1997, approximately 14% of national flood disasters occurred in Quebec. Floods occurring in April and May accounted for up to 40% of the total amount of annual flood events, though floods occurred in every month of the year. Given its dense population, the southern portion of Quebec is particularly vulnerable to flood damage. The Nicolet River was added to a list of spring flood watches issued in early April in 2014 due to higher water level brought on by the spring thaw (CBCnews, 2014).

During the 20th century, increases in annual mean temperature from 0.5℃ to 1.5℃ and in annual precipitation from 5% to 35% have been recorded in southern Canada (Zhang et al., 2000). An analysis of Canadian hydrologic trends over the past 30 years suggest an increase in winter streamflow and a decrease in summer streamflow, as well as an earlier occurrence of peak flow (Whitfield and Cannon, 2000; Zhang et al., 2000). According to the Fifth Assessment Report (AR5) of International Panel on Climate Change (IPCC), global mean temperature will continue to increase by 0.3℃-4.8℃ depending on different assumptions of the concentration-derived Representative Concentration Pathways (RCPs) (IPCC, 2013). Under the assumptions of RCP8.5, southern Quebec's mean annual temperature in the mid- to late-21st-century period will exceed the 1986-2005 mean by 2°C.-, whereas under the assumptions of RCP2.6 this change would remain within 2°C. For the same comparison of future and recent-past periods, mean annual precipitation would increase by 10%-20% or 0%-10% under the assumptions of RCP8.5 or RCP2.6, respectively (IPCC, 2013). For a snowmelt-dominated watershed, changes in precipitation may

affect snow accumulation and streamflow, while changes in temperature will mostly likely influence on the timing of snowmelt (Barnett et al., 2005). For a snowmelt-dominated area, it is therefore essential under a changing climate to record and analyse the characteristics of streamflow, particularly during peak flows.

Widely applied to simulate streamflow in the snowmelt-dominated areas, hydrological models with snowmelt modules can be divided into two types: (i) statistical models which describe the hydrological processes based on average catchment conditions, and (ii) physical models which divide the catchment into hydrological response units and calculate hydrological processes independently. Relating land use and climate change inputs directly to the characteristics of stream flow, physical models have important applications in the modelling and prediction of climate change's effects on stream flow. However, physical models often include parameters which cannot be measured conveniently and must be arrived at through the calibration and validation of the model against historical data (Zhang et al., 2008). This allows the model to accurately represent the study area's physical and hydrological characteristics, making it a reasonably effective tool in forecasting the long-term streamflow under various climate conditions.

The use of the Soil and Water Assessment Tool (SWAT) is warranted in this study given:

i. its solid conceptual and physical foundations in modelling the hydrological response of large and heterogeneous watersheds;
ii. the wide availability of input data (temperature and precipitation); and
iii. its generally good model performance in simulating stream flow resulting from rainfall and snowmelt.

Developed by the United States Department of Agriculture (USDA), SWAT has been widely tested and proven to be an ideal tool for simulating streamflow resulting from rainfall and

snowmelt. The SWAT model uses a temperature index method to simulate snowmelt. In evaluating the SWAT model's ability to accurately simulate streamflow in Minnesota's Wild Rice River watershed, Wang and Melesse (2005) showed it to perform well in simulating monthly and annual streamflow and satisfactorily in predicting daily streamflow. They further noted that spring streamflow, predominantly the result of snowmelt, was predicted with an acceptable accuracy. Applying the SWAT model to the Outardes Basin in Northern Quebec Troin and Caya (2014) noted a satisfactory model performance (small bias values) for daily and monthly time steps, suggesting that the magnitude and timing of spring-snowmelt-generated peak flow could be accurately simulated with the SWAT model.

Applied in several studies conducted to investigate hydrological responses to climate change in southern Quebec, the SWAT model has shown that climate-induced hydrological changes would include a higher total annual runoff, along with earlier snowmelt and discharge peaks (Gombault et al., 2015; Minville et al., 2008; Shrestha et al., 2012). The SWAT model was also successfully applied in the Pike River watershed, situated near the Nicolet River (Gombault et al., 2015). These authors applied a locally-calibrated version of SWAT, which drew on four future climate projections based on either the Canadian Regional Climate Model (CRCM4) or the Arpege regional climate model, to assess the impacts of climate change on the hydrology of the Pike River watershed. Compared to a baseline period (1971-2000), SWAT predicted that under future (2041-2070) climate scenarios annual and winter streamflow would increase 9-19% and 200-300%, respectively. Moreover, SWAT simulations showed significant differences in spatial and seasonal hydrological changes arising from different climate change scenarios and their contrasting assumptions regarding temperature and precipitation shifts.

While previous studies have mainly focused on the combined effects of temperature and precipitation on peak flow (Gombault et al., 2015; Minville et al., 2008; Shrestha et al., 2012), no studies have addressed the independent effects of temperature and precipitation on peak flow. However, it is important to separately elucidate the effects of altered temperature and precipitation patterns on snowfall and snowmelt, as they may affect different hydrological processes, thereby influencing streamflow jointly and separately.

1.2 Objectives

The objectives of this study were twofold:

i. to evaluate the ArcSWAT model's ability to simulate Nicolet River streamflow, and
ii. to predict the impacts of climate change on the Nicolet River watershed's hydrological variables (i.e. annual flow, seasonal flow and peak flow) using a validated model drawing on eleven climate scenarios provided by the North American Regional Climate Change Assessment Program (NARCCAP).

This research particularly focused on the impacts of climate change on future snowfall and snowmelt. Moreover, the separated effects of the projected changes in temperature and precipitation were studied in greater depth than in previous studies. Ultimately, the response to climate changes observed in streamflow characteristics, including annual and seasonal streamflow, as well as peak flow, are discussed.

1.3 Thesis Outline

The organization of this thesis follows the structure of the above-cited objectives. In Chapter 2, a literature review provides an understanding of snowmelt processes and describes the process by which approaches and models used for simulating the snowmelt were selected. In Chapter3, the model was established, calibrated and validated for the Nicolet River watershed. The performance

of the model in simulating streamflow for this watershed was evaluated and discussed. Subsequently, eleven climate change scenarios were applied to the validated model to assess the climate change impacts on the study area's hydrology (Chapter 4). Chapter 5 summarizes the results and draws overall conclusion for the study.

Chapter 2 Literature Review

An important component of the hydrologic cycle in many regions, snowmelt runoff often dominates annual water discharge and can contribute to spring floods. The quantity of snowmelt runoff is related to the snowpack's depth, density and degree of exposure to incoming solar radiation, as well as its rate of melting (Watt, 1989). Ultimately, the rate of snowmelt is controlled primarily by radiant energy (Church, 1988). Several snowmelt-related floods have been caused by a sudden and rapid spring thaw, following significant winter snow accumulation (Institute for Catastrophic Loss Reduction, 2003). While the quantity of snow accumulation in a given watershed, along with the onset and rate of snowmelt within it are affected by weather conditions, each watershed's flood dynamics are uniquely affected by underlying surface conditions. To achieve a quantitative assessment of streamflow and flooding, it is important to understand the hydrological processes of snowmelt, along with the methodology and related techniques for modelling snowmelt.

2.1 Snowmelt theory

Efforts to understand snowmelt hydrology has a long history. Horton (1915) first described the process of snowmelt in the snowpack. Pioneering work on snow hydrology (U.S. Army Corps of Engineers, 1956) introduced comprehensive information regarding snowmelt, and remains widely cited and employed in present research. The work of Anderson (1968) illustrated the possibility of simulating snowmelt, but he also underlined the insufficiency of computing power and the absence of data. Nonetheless, he successfully constructed a snowmelt model using energy balance equations. Subsequently, Gray and Male (1981) demonstrated the integrated physical processes of snowmelt and fully discussed the factors influencing it. In subsequent years, snowmelt theory was gradually developed through many research efforts.

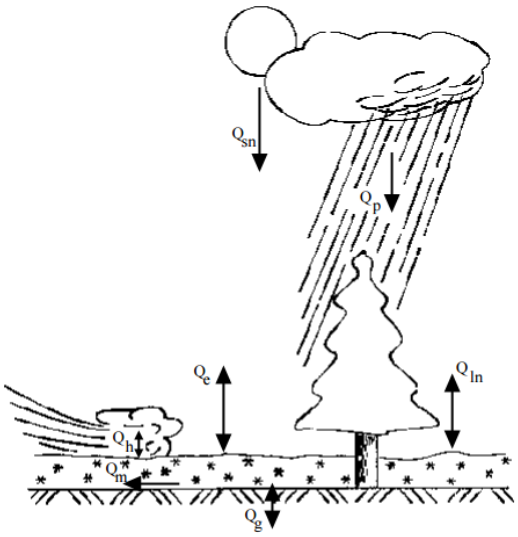

Figure 2-1. Energy fluxes involved in snowmelt and snowpack ablation (Tarboton and Luce, 1996)

Of the energy exchanges occurring during snowmelt (Figure 2-1), changes in radiation flux changes are generally the most important (Tarboton and Luce, 1996). On the Canadian prairies, net radiation exchanges were identified as the major driving force influencing the snowmelt of the continuous snow cover, accounting for up to 93% of snowmelt energy (Gray and O'Neill, 1974). Determined by the balance between incoming and outgoing solar radiation, Q_{sn} is net short-wave (solar) radiation. The amount of incoming solar radiation is a function of multiple factors: latitude, slope, aspect, and albedo, as well as weather conditions (Tarboton and Luce, 1996). While most of the solar radiation incident on the snowpack surface is reflected, a tiny amount is transmitted and absorbed to the deeper layers. However, the penetration of solar radiation through snow can be neglected because its effect on the snowmelt process is limited (Gray and Male, 1981). The net long-wave radiation represents the absorption and emission of long-wave radiation, *i.e.*, black body radiation from the atmosphere and snow surface, respectively. Long-wave radiation from the sky correlates with air temperature and vapor pressure, and is therefore affected by weather and

canopy conditions (Kuz'min, 1961; Brutsaert, 1975; Marks, 1979; Satterlund, 1978). Occurring within 3 meters of the snow surface, turbulent exchange processes consist of sensible heat (Q_h) and latent heat of condensation (Q_e) (Male and Gray, 1981). The temperature gradient, humidity and wind speed are key factors influencing turbulent exchanges. Usually, the ground heat flux Q_g can be neglected compared with radiation exchanges and turbulent exchanges (Bras, 1990). However, over a long period (*e.g.*, a season), the cumulated effect of Q_g cannot be neglected (Male and Gray, 1981). Also having an impact on snowmelt processes, the heat exchanges of liquid water include Q_p (heat brought with rain) and Q_m (heat carried away by melt). Snowmelt theory is the basis of snowmelt modelling methods and modelling techniques.

2.2 Approaches to model snowmelt

There are two basic approaches to simulate the snowmelt processes:

i. temperature-based methods (including degree-day and temperature-index methods) use air temperature as the sole index to calculate the snowpack melting rate, and
ii. energy balance methods which involve many components contributing to snowmelt, including heat and radiation exchanges, sensitive and latent diffusions and the impacts of rain.

2.2.1 Degree-Day Method

A common method used for simulating snowmelt, the degree-day method assumes that a relationship exists between melt rate and positive temperatures. The basic equation for the degree-day method can be written as (Hock, 2003):

$$\sum_{i=1}^{n} M = DDF \sum_{i=1}^{n} T^{+} \Delta t \qquad 2\text{-}1$$

where,

DDF is the degree-day factor

M is the quantity of ice and snow melt,

T^{+} is the sum of air temperatures during the period, and

Δt is a period of n time intervals.

While the time interval for the degree-day method can an hour, day or month, most previous studies have used daily intervals (Hock, 2003). An essential parameter for the degree-day method, the exactitude of *DDF* assessments influences the accuracy of snowmelt simulation. The *DDF* can be computed by either energy balance computations (Arendt and Sharp, 1999) or direct measurements, e.g., lysimetric outflow (Kustas and Rango, 1994) or ablation stakes (Braithwaite et al., 1998). Studies have shown temporal and spatial shifts in *DDF*; for example, estimates of *DDF* for different regions of western China showed an increasing trend from northwest to southeast. Maritime glaciers have a higher *DDF* value than subcontinental or more continental glaciers (Zhang, 2006). Moreover, high altitude areas have a greater *DDF* for snow ablation than low altitude areas (Kayastha, 2000). Some studies have focused on temporal variations in *DDF*; for instance, SNOTEL sites showed an increase in *DDF* over the melt season, which was revealed to be related to the density of forest cover, and other shade-contributing materials (DeWalle, 2002).

2.2.2 Temperature Index Method

The temperature index method is based on the same assumptions as the degree-day method, namely that a correlation exists between the melt rate and positive temperatures. The degree-day

method can be categorized as a temperature index method when the interval periods are hours, minutes or seconds. The basic expression of this relationship is given as (Singh and Kumar, 1996):

$$M = M_f(T_i - T_b) \qquad 2\text{-}2$$

where,

M is the snowmelt generated per unit time (cm T^{-1}),

M_f is the melt factor (cm $°C^{-1}$ T^{-1}),

T_b is the base temperature (usually 0°C), and

T_i is the index air temperature (most commonly the daily maximum or mean daily temperature),

However, the temperature is not the only factor affecting melt rate. To identify further factors affecting the melt rate, Yoshida (1962) measured the water equivalent of snow at five stations in Japan, concluding that the melt factor may be different at sites receiving varying exposure to solar radiation. Further, Eggleston et al. (1971) suggested that the melt factor was determined by a proportionality constant, vegetation transmission coefficient, solar radiation index and snow albedo. Among these factors, the solar radiation index varies with latitude, slopes and aspect. Having conducted a series of measurements of air and canopy temperature in coniferous forests under different cover densities, insolation and latitude, Pomeroy (2009) found that air temperature did not always match canopy temperature. He attributed this to the fact that short-wave radiation flux and the flux of latent heat were not directly related to air temperature and exhibited wide variations depending on the weather conditions. The temperature difference was greatest in regions of discontinuous canopy under strong insolation. Due to wide variations in forest cover, Pomeroy (2009) found maximum values of M_f to be 2- to 12-fold greater than the minimum values of M_f . Ultimately, all these studies focused on melt rate contributed to a more sophisticated temperature index method for snowmelt modelling.

2.2.3 Energy Balance Approach

The snowmelt processes are predominantly controlled by energy exchanges between the atmosphere and the snowpack. According to Gray and Male (1981), the amount of energy available for snowmelt can be expressed as:

$$Q_m = Q_{sn} + Q_{ln} + Q_h + Q_e + Q_g + Q_p - \frac{dU}{dt} \quad \text{2-3}$$

where,

Q_e is the flux of the latent heat (evaporation, sublimation, condensation) at the snow-air interface,

Q_g is the flux of the heat from the snow ground interface by conduction,

Q_h is the convective or sensible heat flux from the air at the snow-air interface,

Q_{ln} is the net long-ware radiation flux at the snow-air interface,

Q_m is the energy flux available for melt,

Q_p is the flux of heat from rain,

Q_{sn} is the net short-ware radiation flux absorbed by the snow, and

dU/dt is the rate of change of internal (or stored) energy per unit area of snowcover.

To implement an energy balance approach, adequate meteorological data, snowpack measurements and high-performance computers are required. However, compared with temperature index methods, energy balance method involves relatively complicated energy exchange processes. Accordingly, many efforts were made to generate an algorithm of the energy balance. Early work by Wilson (1941) discussed some principles of thermodynamics that apply to the ripening and melting of snow. More integrated work by The U.S. Army Corps of Engineers (1956) illustrated the snowmelt's physical processes and applied a model to simulate snowmelt; however, several inaccuracies remained. Anderson and Crawford (1964) were the first to explore the possibility of simulating continuous snowmelt runoff using a computer-based method

combining the temperature index and energy balance methods, along with the Stanford Watershed Model (SWM). Later, some studies conducted by Anderson (1968) led to the development of a snowmelt equation for improving continuous energy balance computational techniques. Subsequently, the energy balance method was widely used as a primary or secondary method in model snowmelt modules. Anderson's point energy balance model (Anderson, 1976), the SHE model (Morris, 1982), the Utah State University simulation model (USUWSM) (Leu, 1988), the snow component of the USGS Precipitation-Runoff Modeling System (PRMS) and WEPP model (Leavesley et al., 1987; Young et al., 1989) were predominantly based on the energy balance method which emphasizes physical processes.

2.3 Models for snowmelt modelling

The complexity of snowmelt hydrology has led to widespread applications of snowmelt equations in comprehensive hydrological models (Rango and Martinec, 1995). Snowmelt simulation methods and data requirements for four widely used models are summarized in Table 2-1. While the energy balance method was applied in the UEB model, the remaining models implemented the temperature index method. Among them, the SWAT model operates with a greater number of variables to allow an accurate simulation the snowmelt based on local weather conditions. Moreover, the SWAT variables can be further modified by climate change factors to assess potential climate change impacts on snowmelt and hydrology.

Table 2-2 illustrated the features of the four models in simulating snowmelt. Open-source models are preferable, because they are available to the public for use or modification from their original design. In contrast, point scale models and lumped models are not capable of considering different land use or soil types (Ghavidelfar et al., 2011). However, fully-distributed models often cannot be applied at a watershed scale area due to a lack of accessibility to the

necessary data. Accordingly, semi-distributed models are a reasonable compromise in overcoming the problems of lumped and fully-distributed models, which divide the watershed into small individual units. Among three semi-distributed models, SWAT was prioritized as it considers an areal depletion curve when calculating snowpack depletion, and can be applied to flood protection.

When considering a hydrological model, the catchment's physical characteristic and availability of data inputs should be considered. The Nicolet River watershed is a watershed scale area for which land use, soil type and weather data are available. In undertaking the present research, the author sought to evaluate the impacts of climate change on peak flow and streamflow in the Nicolet River watershed. Within the study area, peak flows were predominately contributed by the snowmelt and could lead to spring floods. Thus, a sophisticated snowmelt component was a priority in selecting a model, and the inclusion of a flood protection function was preferable. Successfully applied to southern Quebec's Pike River (Gombault et al., 2015), SWAT was confirmed as being a reasonably accurate tool for simulating the streamflow in that region. Moreover, SWAT is a comprehensive model, which includes hydrology simulations including surface runoff, evapotranspiration, soil water, groundwater, as well as nutrient and pesticide simulations. The Nicolet river is vulnerable to contamination by pesticides as the land is used for large-scale agricultural production. Though the present study does not focus on water quality analysis, the SWAT was initially chosen for this research as it contains nutrients and pesticide components, which may helpful to further model application and development.

Table 2-1 Snowmelt simulation methods and data requirements for four models

Model	Approach		Data Inputs						
	Temperature Index Method	Energy Balance Method	Precipitation	Temperature	Wind speed	Relatively humidity	Solar radiation	Albedo	snowmelt parameters
HBV	√		V	V					C
SHE	√		V	V					V
UEB		√	V	V	V	V	V	V	
SWAT	√		V	V	V	V	V	V	V

Note: The method which is adopted by model (√); variable parameters of simulation (V); constant parameters of simulation (C).

Table 2-2 Features of four models for snowmelt simulation

Model	Access to program	Original application		Snow model spatial extent			Areal extent of snowmelt		Potential application to flood protection	Reference
		Urban	Non-urban	point scale	lumped	semi-distributed	Catchment discretization	Areal depletion curve		
HBV	Public		√		√	√	√		√	(Seibert, 2005)
SHE	Proprietary		√		√	√	√		√	(Graham and Klide, 2002)
UEB	Public		√	√						(Tarboton and Luce, 1996)
SWAT	Public	√	√		√	√	√	√	√	(Neitsch et al., 2011)

Note: An attribute which is considered by model (√);

Chapter 3 Hydrological Modelling of southern Quebec's Nicolet River Watershed

3.1 Abstract

As snowmelt runoff is responsible for peak flow in the snowmelt-dominated Nicolet River watershed, spring floods may occur when the temperature rises rapidly over a short time. Changing winter and spring climatic patterns will induce the changes in streamflow, with rising temperatures engendering greater winter runoff and lesser snow accumulation. Recent years, have seen an increase in the magnitude and frequency of large-scale winter flood events in the Nicolet River watershed; for example, in 2014, Hydro Quebec declared the Nicolet River to be at a flood warning stage. Once calibrated for the Nicolet River watershed, the ArcSWAT model was subjected to sensitivity analysis. This indicated CN_2, GW_REVAP, ESCO, SLSOIL and SOL_AWC to be the most sensitive parameters in streamflow simulation, while the volume of peak flow changes dramatically with the snow-related parameters SFTMP, SMTMP, SMFMX and SMFMN. Calibrated and validated against the observed data for 1986-1990 and 1991-2000, respectively, the model showed good performance in simulating monthly streamflow and a satisfactory performance for daily streamflow: $|PBIAS| < 15\%$, Nash-Sutcliffe efficiency (NSE) > 0.50 and RMSE-observations standard deviation ratio (RSR) < 0.70 across both model calibration and validation. While ArcSWAT proved to be a generally reliable tool in simulating streamflow, accurately simulating the timing of peak flows, it slightly underestimated peak flow volume.

3.2 Introduction

A key component of the hydrologic cycle in snowmelt-dominated watersheds, snowmelt runoff dominates large discharge events and may trigger spring floods. According to the Emergency Preparedness Canada (EPC) electronic disaster database, over 65% of the flood disasters are

caused by snowmelt runoff, storm water, or storm rainfall runoff (Brooks et al., 2001). Though floods in the watershed under study occurred throughout the year, they predominantly (40%) occurred in April and May. The amount of snowmelt runoff is related to the depth, density and degree of exposure of the snowpack, as well as the rate of melting (Ward, 1989). Both the amount of snow accumulation and the snowpack's melt rate are affected by weather conditions. Given the regional character of snowmelt, floods commonly influence multiple watersheds.

Southern Quebec is vulnerable to flood damage because of its dense population. Recently, higher water level during the spring thaw have extended flood watch regions in Quebec. The handful of studies conducted on the Nicolet River have mainly emphasized water quality issues; for example, Caux et al. (1996) used the CREAMS model to simulate pesticide movement in the Nicolet river. Likewise, Quémerais et al.(1994), who focused on polychlorinated biphenyls (PCBs) in the St. Lawrence River system, noted that PCBs levels in the Nicolet River peaked during the spring freshet and were mostly in the dissolved phase. Concentrating on minor and trace element concentrations in the St. Lawrence River, Rondeau et al. (2005) found the Saint Lawrence River's south shore tributaries, including the Nicolet River, to show high metal concentrations due to anthropogenic activities in their basins. A comparison of inter-annual variability in heavy spring floods within the St. Lawrence River watershed conducted by Mazouz et al. (2012), showed the frequency of spring floods to have increased between 1930 and 2010, while the variance in the timing of heavy spring floods in the Nicolet SW River watershed decreased significantly over the same period. In 2014, Hydro Quebec declared the Nicolet River to be at a flood warning stage (CBCnews, 2014).

Hydrological modelling is a reliable approach to capturing a catchment's hydrological characteristics and simulating the hydrological response under an altered future climate. For the

Nicolet River watershed, where snowfall is the dominant form of precipitation in winter and the annual peak flow generally occurs during the spring snowmelt, a snowmelt component will be essential requirement in selecting a model capable of simulating streamflow during this period. There are two basic approaches to simulate snowmelt processes: temperature index and energy balance methods. Early snowmelt models used a temperature index approach which implemented a monthly melt factor (World Meteorological Organization (1986), while later operational runoff models [e.g., HBV (Bergstrom, 1976); SRM (Martinec and Rango, 1986); SHE (Bøggild et al., 1999), ArcSWAT (Arnold et al., 1998)] have generally based their snowmelt modules on the temperature index method (Hock (2003)).

The ArcSWAT model (Arnold et al., 1998), a comprehensive river basin and watershed model particularly well-suited to modelling continuous long-term hydrological events provides different modules addressing different user demands, *e.g*., weather, surface runoff, percolation, evapotranspiration, snowmelt. Using the temperature index method to simulate snowmelt processes, ArcSWAT's snowmelt module successfully modelled snowmelt-driven streamflow at daily or monthly intervals in a number of locales: Taleghan Mountain watershed (NW Iran — (Noor et al., 2014); Outardes basin (Troin and Caya, 2014); Blue River watershed (Lemonds and McCray, 2007); Ontonagon River basin (Wu and Johnston, 2007). These studies laid a solid foundation for model application.

The main objectives of the work reported in this chapter were: (i) to prepare the ArcSWAT model for the Nicolet River watershed in southern Quebec; (ii) to conduct a sensitivity analysis, model calibration (1986-1990) and model validation (1991-2000); (iii) to evaluate the performance of the ArcSWAT model in simulating streamflow on a monthly and daily time step.

Along with enumerating the study area's characteristics, this chapter's Section 3, will the model input requirements and the evaluation methods used for model calibration and validation. In Section 4, the ArcSWAT model will be adjusted and supplied data regarding the study watershed's physical characteristics. The model will then be calibrated and validated for streamflow. In addition, based on a comparison of the model's output to measured streamflow, the ArcSWAT model's performance in modelling the study area's streamflow will be assessed and discussed.

3.3 Materials and Methods

3.3.1 Site Description

The research area was located within southern Quebec's Nicolet River watershed. Originating in Lake Saint-Pierre, the Nicolet River flows through the towns of Victoriaville and Warwick on its way to becoming a south shore tributary of the Saint Lawrence River (Figure 3-1). Stream flow data from hydrological station 02OD003 was downloaded from Environment Canada's HYDAT database. While the Nicolet River drains a watershed of approximately 3380 km^2, the 02OD003 station only monitors a 1764 km^2 portion of that area (36°04'—36°21' N lat. 50°38'—51°12' E long.) Weather data, including precipitation and temperature, were downloaded from four meteorological stations (Climate ID: 701HE63; 7027783; 7022160; 7027248) situated within the watershed (Figure 3-1).

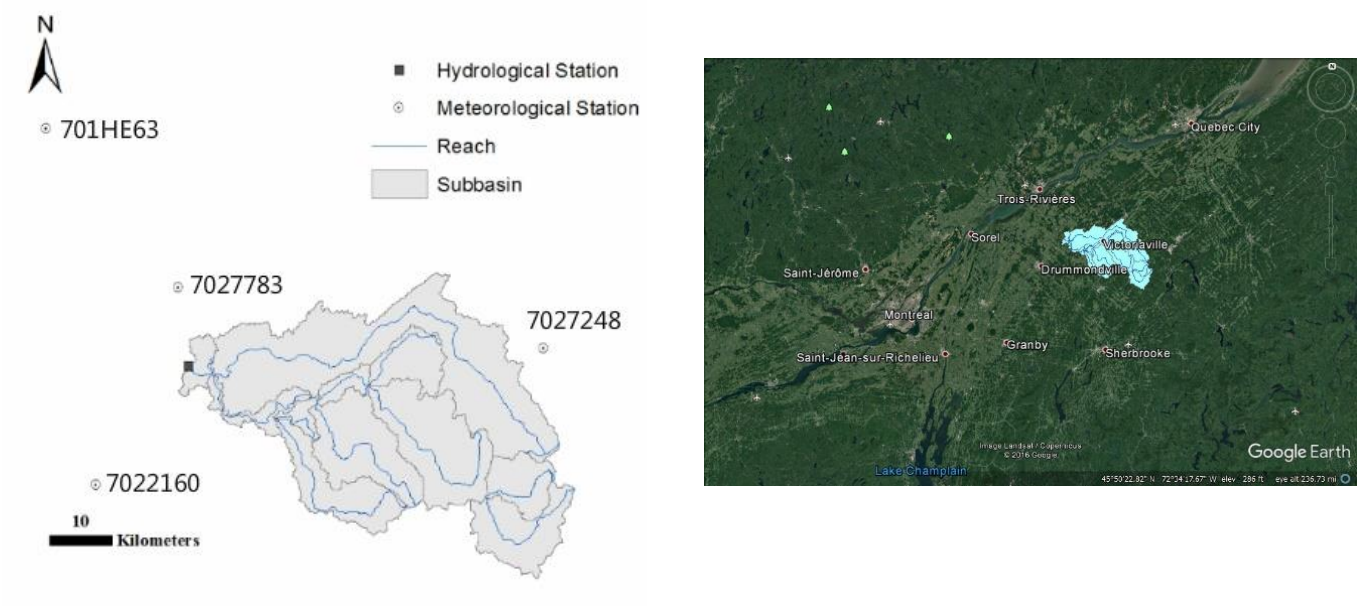

Figure 3-1: Map of Nicolet watershed in southern Quebec, Canada (Weather stations: Trois River (701HE63); St Wenceslas (7027783); Drummondville (7022160); St Ferdinand (7027248). Hydrological station: NICOLET (RIVIERE) À 5,8 KM EN AVAL DE LA RIVIERE BULSTRODE (ID: 02OD003))

The 30-year (1981-2010) Canadian Climate Normal Statistics for the four weather stations selected to provide weather inputs are shown in Figure 3-2. Based on the St Ferdinand weather station (Climate ID: 7027248), the study area's average daily temperature was 4.4 °C. Generally, the temperature remains below 0°C from November onward, then shifts back above 0°C in March. The study area's annual average precipitation was 1227.7mm, of which 76.5% was rainfall and 23.5% snowfall.

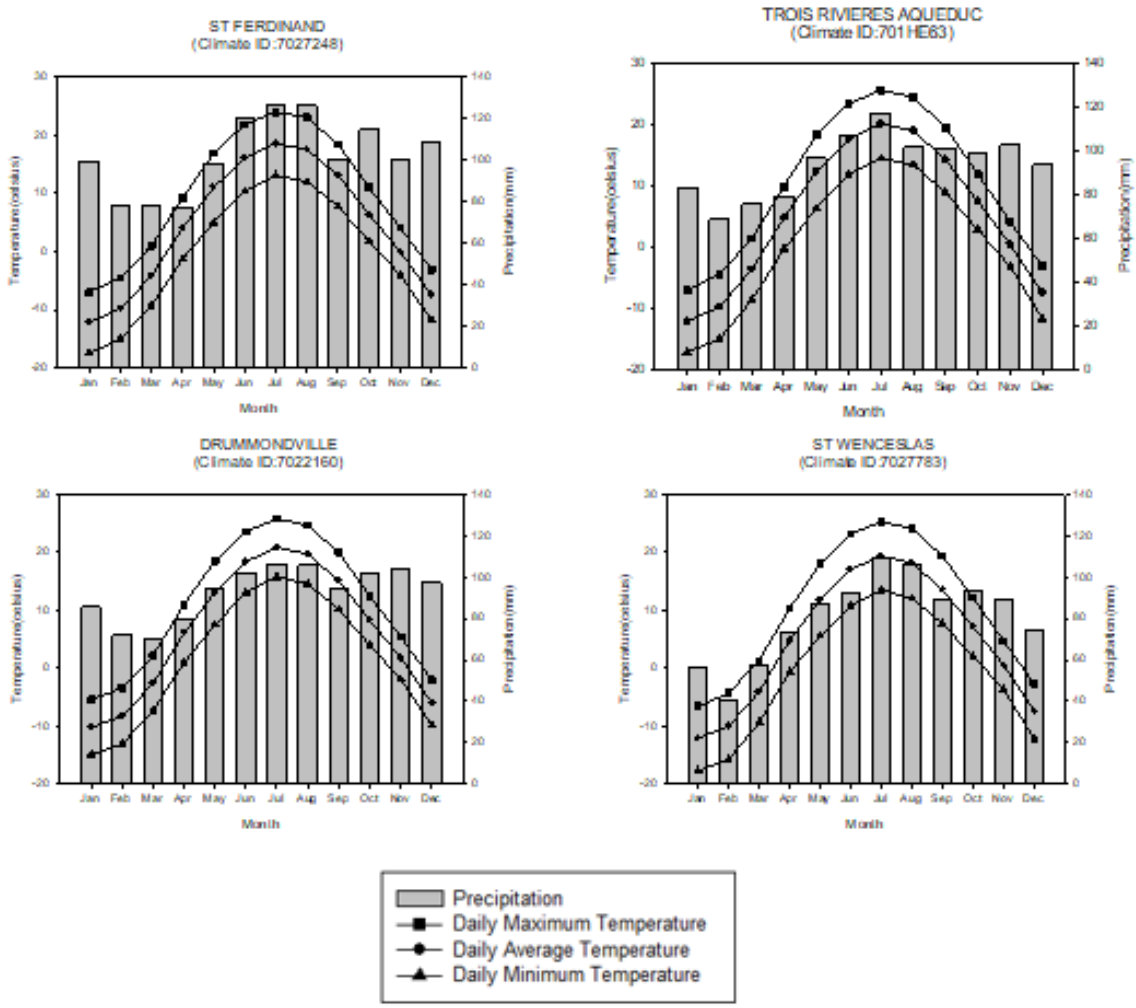

Figure 3-2: The 30-year (1981-2010) Canadian Climate Normal Statistics for the weather stations in the study area

3.3.2 Model Description

3.3.2.1 Overview of ArcSWAT

ArcSWAT, an ArcGIS extension and graphical user input interface for the Soil and Water Assessment Tool (SWAT) (Neitsch et al., 2011), was employed to simulate streamflow in this study due to its comprehensive capacity of hydrologic simulation. SWAT is suitable to modelling streamflow for the study area, as it has been widely and successfully applied in snowmelt-dominated locations (Lemonds and McCray, 2007; Noor et al., 2014; Wu and Johnston, 2007). Moreover, the model was successfully applied to modelling the Outardes basin (Troin and Caya, 2014) and the Pike River watershed (Gollamudi, 2006), both situated in southern Quebec.

A physical-based, continuous, watershed-scale model, SWAT was developed by the United States Department of Agriculture (USDA). Spatially distributed data on topography, soils, land use, and meteorology are required for the model to simulate hydrological processes. The modelled watershed was divided into multiple sub-basins based on digital elevation data, then further subdivided into hydrologic response units (HRUs) depended on soils, land use and slope features. Driven by the water balance, the ArcSWAT model can compute a wise range of hydrologic processes: precipitation, surface and subsurface flow, evapotranspiration, infiltration, snow accumulation and snowmelt. The general sequence of processes used by ArcSWAT to model the land phase of the hydrologic cycle in the present study is shown in Figure 3-3. Simulating a watershed's hydrology occurs in two phases:

(i) the hydrological phase, which controls the amount of water entering different sub-basins' main channels according to the water balance equation (Neitsch et al., 2011):

$$\theta_{\mathrm{t}} = \theta_0 + \sum_{\mathrm{i=1}}^{\mathrm{i=t}} (\mathrm{R_{day}}_i - \mathrm{Q_{surf}}_i - \mathrm{ET_a}_i - \mathrm{w_{seep}}_i - \mathrm{Q_{gw}}_i) \qquad 3\text{-}1$$

where,

t is the time (days),

$\mathrm{w_{seep}}_i$ is the quantity of water entering the vadose zone from the soil profile on day *i* (mm),

$\mathrm{ET_a}_i$ is the quantity of evapotranspiration on day *i* (mm),

$\mathrm{Q_{gw}}_i$ is the quantity of return flow on day *i* (mm H_2O),

$\mathrm{Q_{surf}}_i$ is the quantity of surface runoff on day *i* (mm),

$\mathrm{R_{day}}_i$ is the quantity of precipitation on day *i* (mm),

θ_0 is the initial soil water content (mm), and

θ_{t} is the final soil water content (mm).

(ii) the second, routine phase of the hydrologic cycle phase, begun once the loading of water to the main channel is determined, involves the loading of the watershed through the stream network.

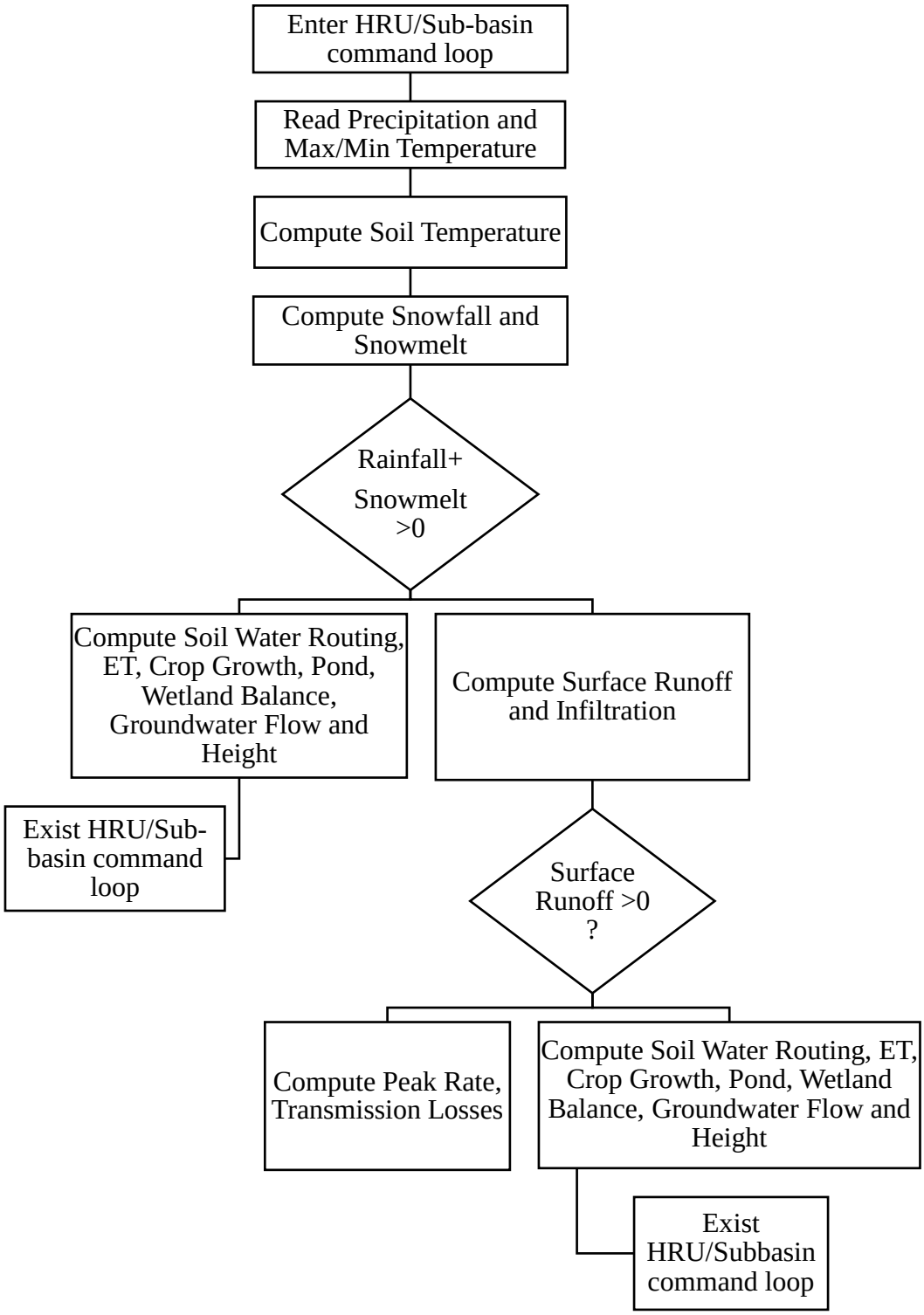

Figure 3-2: The land phase of the hydrologic cycle as simulated in this study

When precipitation occurs on a given hydrological response unit (HRU), it may be intercepted by the vegetation canopy or fall to the surface. The surface water subsequently infiltrates into soil layers or generates overland flow. In ArcSWAT, the curve number method first estimates the quantity of surface runoff, then assumes that the remaining water will infiltrate the soil and contribute to streamflow by underground pathways, or evaporate from the soil surface. The curve number method of surface runoff estimation is based on SCS runoff equations developed for various land uses and soil types (Williams and LaSeur, 1976):

$$Q_{surf} = \frac{(R_{day} - I_a)^2}{(R_{day} - I_a + S)} \quad 3\text{-}2$$

where,

I_a represents the initial abstractions, including surface storage, interception and infiltration prior to runoff (mm),

Q_{surf} is the accumulated runoff or rainfall excess (mm),

R_{day} is the rainfall depth for the day (mm H_2O),

S is the retention parameter (mm) which is determined soil type, land use, management and slope.

As I_a is commonly approximated as 0.2S, Eq. 3-2 becomes:

$$Q_{surf} = \frac{(R_{day} - 0.2S)^2}{(R_{day} + 0.8S)} \quad 3\text{-}3$$

where,

$$S = 25.4\left(\frac{100}{CN} - 10\right) \quad 3\text{-}4$$

where,

CN is the curve number for the day.

Evapotranspiration (ET) represents a major constituent of the hydrologic unit's water balance in ArcSWAT. The model employs the Penman-Monteith method to calculate potential evapotranspiration (ET_p). Once ET_p is determined, the actual evaporation (ET_a) is determined by a method similar to that of Richtie (Ritchie, 1972), which first calculates the evaporation of intercepted rainfall, then estimating the maximum quantity of transpiration and sublimation, as well as soil evaporation. Finally, the actual quantity of sublimation and soil evaporation are calculated for the watershed. The actual soil evaporation is determined from soil depth and soil water content (θ) through exponential functions, while transpiration by the vegetation is estimated from ET_p and leaf area index (LAI) through a linear function.

The lateral flow is simulated by a kinematic storage model for each soil layer which accounts for the variation in conductivity, slope and θ. The volume of water of lateral flow per day is given as (Neitsch et al., 2011):

$$Q_{lat} = 0.024\left(\frac{2 \cdot SW_{ly,xs} \cdot k_{sat} \cdot slp}{\emptyset_d \cdot L_{hill}}\right) \qquad 3\text{-}5$$

where,

k_{sat} is the saturated hydrologic conductivity (mm h^{-1}),

slp is the elevation per unit distance or slope (m m^{-1}),

L_{hill} is the hillslope length (m),

Q_{lat} is the quantity of lateral flow per day (mm d^{-1}),

$SW_{ly,xs}$ is the water stored in the saturated zone of the hillslope per hydrological unit (mm), and

$\emptyset_d$ is the porosity of the soil layer at field capacity (θ_{fc}) given in mm mm^{-1}

Water recharging from lowest soil layers can discharge into the streamflow as groundwater or baseflow. In ArcSWAT, the groundwater is calculated as (Neitsch et al., 2011):

$$Q_{gw_i} = 800\mu \cdot \alpha_{gw} \cdot h_{wtbl} \quad 3\text{-}6$$

where,

h_{wtbl} is the water table depth (m),

Q_{gw_i} is groundwater flow into the main channel on day *i* (mm),

α_{gw} is the baseflow recession constant, and

μ is the specific yield of the shallow aquifer (m m^{-1}).

In ArcSWAT, the snow accumulation is represented by the increase in snowpack water content. ArcSWAT judges precipitation to be rain or snow according to the mean daily air temperature. The snowfall temperature, given by the user, below which precipitation is classified as snowfall and the water equivalent of snowfall is added to the snowpack. The mass balance equation for the is given as:

$$SNO_i = SNO_{i-1} + R_i - E_{sub_i} - SNO_{mlt_i} \quad 3\text{-}7$$

where,

E_{sub_i} is the quantity of sublimation on a given day *i* (mm),

R_i is the quantity of snowfall on a given day *i* (mm),

SNO_i and SNO_{i-1} are the snowpack water for a given day and the day before (mm), respectively, and

SNO_{mlt_i} is the quantity of snow melt on a given day *i* (mm).

The SWAT snowmelt module employed the temperature-index method to estimate snowmelt. The method assumes a linear relationship between the snowmelt and the difference between average maximum temperature and a threshold temperature. The timing and quantity of

snowmelt are determined by the combination of snowpack temperature, melting rate and the areal coverage of snow. Snowmelt is included with rainfall in calculating the runoff and infiltration (Neitsch et al., 2011):

$$SNO_{mlt} = b_{mlt} \cdot sno_{cov} \cdot \left[\frac{T_{snow} + T_{mx}}{2} - T_{mlt}\right] \quad 3\text{-}8$$

$$b_{mlt} = \frac{b_{mlt6} + b_{mlt12}}{2} + \left[\frac{b_{mlt6} - b_{mlt12}}{2} \cdot \sin\left(\frac{2\pi}{365}[d_n - 81]\right)\right] \quad 3\text{-}9$$

where,

b_{mlt} is the melt factor for the day (mm d^{-1} °C^{-1}),

b_{mlt6} is the melt factor for June 21 mm d^{-1} °C^{-1}),

b_{mlt12} is the melt factor for December 21 (mm d^{-1} °C^{-1}),

d_n is the n^{th} day of a year,

sno_{cov} is the fraction of the HRU area covered by snow,

SNO_{mlt} is the amount of snow melt on a given day (mm),

T_{mlt} is the threshold temperature above which snow melt is allowed (℃),

T_{mx} is the maximum air temperature on a given day (℃),

T_{snow} is snow pack temperature on a given day (℃).

Due to the differences in topography and shape for each sub-basin, the distribution of snowpack will rarely be uniformly within a watershed; however, factors influencing the distribution of snowpack, such as topography and shape, are usually similar during a given period of time. Thus, the areal coverage of snowpack in an HRU can be represented by the amount of snow. This correlation can be presented by the depletion curve number method (Neitsch et al., 2011):

$$sno_{cov} = \frac{SNO}{SNO_{100}} \cdot \left[\frac{SNO}{SNO_{100}} + e^{(cov_1 - cov_2) \cdot \frac{SNO}{SNO_{100}}}\right]^{-1} \quad 3\text{-}10$$

where,

cov_1 and cov_2 are coefficients that define the shape of the curve. Their values are determined by solving the Eq. 2-10 with two known points: 95% coverage at 95% SNO_{100} and 50% coverage at a user specific fraction of SNO_{100}, and

SNO_{100} is the threshold depth of snow at 100% coverage (mm),

However, it is important to note that the depletion curve affects snowmelt only when $0 \leq SNO \leq SNO_{100}$; once $SNO > SNO_{100}$, the snow cover in the HRU is regarded as uniform.

3.3.2.2 Description of Parameters

Among the model's key parameters, the initial runoff curve number for moisture condition II (CN2) determines the soil permeability, land use, and antecedent soil water conditions. This parameter also directly decides the water available for runoff and infiltration (Eq. 3-2, 3-3, and 3-4). For a given rainfall intensity, the generation of runoff increases with an increase in CN2. The range of CN2 values suggested by the handbook (Arnold et al., 2012a) is between 74 and 86. While the volume of surface runoff is controlled by CN2, the timing of surface runoff concentration changes follows the surface runoff lag coefficient (SURLAG). For a given time of concentration, more water is held in storage as SURLAG decreases, which means the release of surface runoff will be delayed and the simulated streamflow hydrograph will be smoother.

A major ArcSWAT parameter, ET correlates strongly with all hydrologic components of the water balance. The ET is most strongly influenced by the soil evaporation compensation factor (ESCO), and Groundwater "revap" coefficient (GW_REVAP). Ranging from 0.01 to 1, ESCO is included to allow the user to modify the depth distribution used to meet the soil evaporative demand. The model can extract more water to meet the evaporative demand from lower layers if the value of ESCO is reduced, as expressed in Eq. 3-11 (Neitsch et al., 2011):

$$E_{soil,ly} = E_{soil,zl} - (E_{soil,zu} \cdot ESCO) \quad 3\text{-}11$$

where,

$E_{soil,y}$ is the evaporative demand for soil layer ly (mm),

$E_{soil,zl}$ is the evaporative demand at the lower boundary of the soil layer (mm), and

$E_{soil,zu}$ is the evaporative demand at the upper boundary of the soil layer (mm).

Ranging between 0 and 1, the Groundwater "revap" coefficient (GW_REVAP), represents the water moving from shallow aquifers into the overlying unsaturated zone. If water is removed from the capillary fringe by evaporation, it will be replaced by water from the underlying aquifer; water may then be further removed by deep-rooted plants. As GW_REVAP increases, the rate of water transferring from the shallow aquifer to root zone approaches the rate of ET_p, indicating that more water can be shifted from the shallow aquifer to the root zone to meet the evaporative need., The baseflow recession factor ALPHA_BF (d^{-1}) is a direct index of groundwater flow response to recharge, and controls the groundwater level (Eq. 2-5). The greater the ALPHA_BF value, the lower is the baseflow value for the summer period. While $0.1 \leq$ ALPHA_BF ≤ 0.3 is suggested for an area with the slow response to recharge, $0.9 \leq$ ALPHA_BF ≤ 1.0 are recommended for an area with a rapid response. The magnitude of lateral subsurface flow (SL_SOIL) is affected by slope length (e.g. Eq. 3-5).

The overland flow time of concentration (t_{ov}) is influenced by Manning's "n" value for the tributary channels [CH_N(1)], average slope length (SLSUBBSN) and slope of sub-basin (SLOPE). Increasing CH_N(1) and SLSUBBSN or decreasing SLOPE would therefore result in the reduction of concentration time. Time of concentration in the present study was given as (Neitsch et al., 2011):

$$t_{ov} = \frac{L_{slp}^{0.6} \cdot n^{0.6}}{18 \cdot slp^{0.3}} \quad 3\text{-}12$$

where,

n is Manning's "n" value for the tributary channel,

t_{ov} is the overland flow time of concentration (m s^{-1}), and

L_{slp} is the average slope length (m).

Snow accumulation and snowmelt processes are mainly controlled by snowfall temperature (SFTMP), snow melt base temperature(SMTMP), melt factor for snow on June 21(SMFMX), melt factor for snow on December 21(SMFMN), minimum snow water content that corresponds to 100% snow cover(SNOWCOVMX) and fraction of snow volume represented by SNOCOVMX that corresponds to 50% snow cover(SNO50COV). The snowfall temperature (SFTMP), the threshold temperature above which snowmelt is allowed, serves to discriminate precipitation between rainfall and snowfall. When the mean daily air temperature of a given day exceeds SFTMP, precipitation falls as snowfall and is stored in the snowpack (e.g., Eq. 3-8). The value of SFTMP should be set between 5℃ and 5 ℃. The melt factor for snowmelt, namely the amount of water (mm) melted per unit of temperature (in ℃) in a day, is determined by the melt factor for snow on June 21(SMFMX), and the melt factor for snow on December 21(SMFMN), as shown in Eq. 3-9. The ranges of the SMFMX and SMFMN are both set between 1.4 and 6.9 m d^{-1} °C^{-1}) in rural areas. The SNOWCOVMX parameter is used to define the threshold depth of snow at 100% coverage (mm) and functions as SNO_{100} in Eq. 3-9. If the water content of the snow pack on a given day is below SNOWCOVMX, the fraction of the HRU area covered by snow must be recalculated by Eq. 3-10. If the value of SNOWCOVMX decreases, the impact of the areal depletion curve on snow melt will be minimized. The value of SNO50COV, which varies between 0.01 and 0.99, is used to

calculated the fraction of the HRU area covered by snow by determining the values of cov_1 and cov_2 (Eq. 3-10).

3.3.3 Model Input

Datasets required by ArcSWAT model consist in a digital elevation model (DEM), soil type, land use, temperature and precipitation data.

3.3.3.1 Geographical Data

A 90 m resolution DEM was acquired from the CGIAR Consortium for Spatial Information (CGIAR-CSI), originally provided by the NASA Shuttle Radar Topographic Mission (SRTM). The DEM raster files were merged and were projected to UTM Zone 19N with datum WGS 1983. The watershed boundary and stream network were generated by the automatic watershed delineation tool in ArcSWAT, based on the DEM. Land use was accessed from the WaterBase database, and resampled at a resolution of 800 m was applied to the study area. Hay (HAY), Forest-Mixed (FRST), Wetland-Non-Forested (WETN) were identified as dominant land uses. The soil information was drawn from an FAO-UNESCO soil map using a different nomenclature and classification than the model. However, no matter what kind of database is applied, the soil can be classified into four types depending on Soil Conservation Service (SCS) system. Accordingly, different soil physical and chemical properties could be identified for four soil types, e.g., bulk density (ρ), saturated hydraulic conductivity (k_{sat}), soil texture etc. In the study area, two types of soil (Po13-2a-4964 and Po10-2b-3458) were most prevalent; both were loam soils and belonged to class C (Table 3-1), indicating a slow infiltration rate, slow rate of water transmission and a high runoff potential.

Table 3-1: The definitions for the different soil hydrologic groups

Soil Hydrologic Group	Definitions
A	Soil having high infiltration rates even when thoroughly wetted, consisting chiefly of sands or gravel that are deep and well to excessively drained. These soils have a high rate of water transmission.
B	Soil having moderate infiltration rates when thoroughly wetted, chief moderately deep to deep, moderately well to well drained, with moderately fine to moderately coarse texture. These soils have a moderate rate of water transmission.
C	Soil having slow infiltration rates when thoroughly wetted, chiefly with a layer that impedes the downward movement of water or of moderately fine to fine texture and a slow infiltration rate. These soils have a slow rate of water transmission (high runoff potential)
D	Soils having very slow infiltration rates when thoroughly wetted, chiefly clay soils with a high swelling potential; soils with a high permanent water table; soils with a clay pan or clay layer at or near the surface; and shallow soils over nearly impervious materials. These soils have a very slow rate of water transmission.

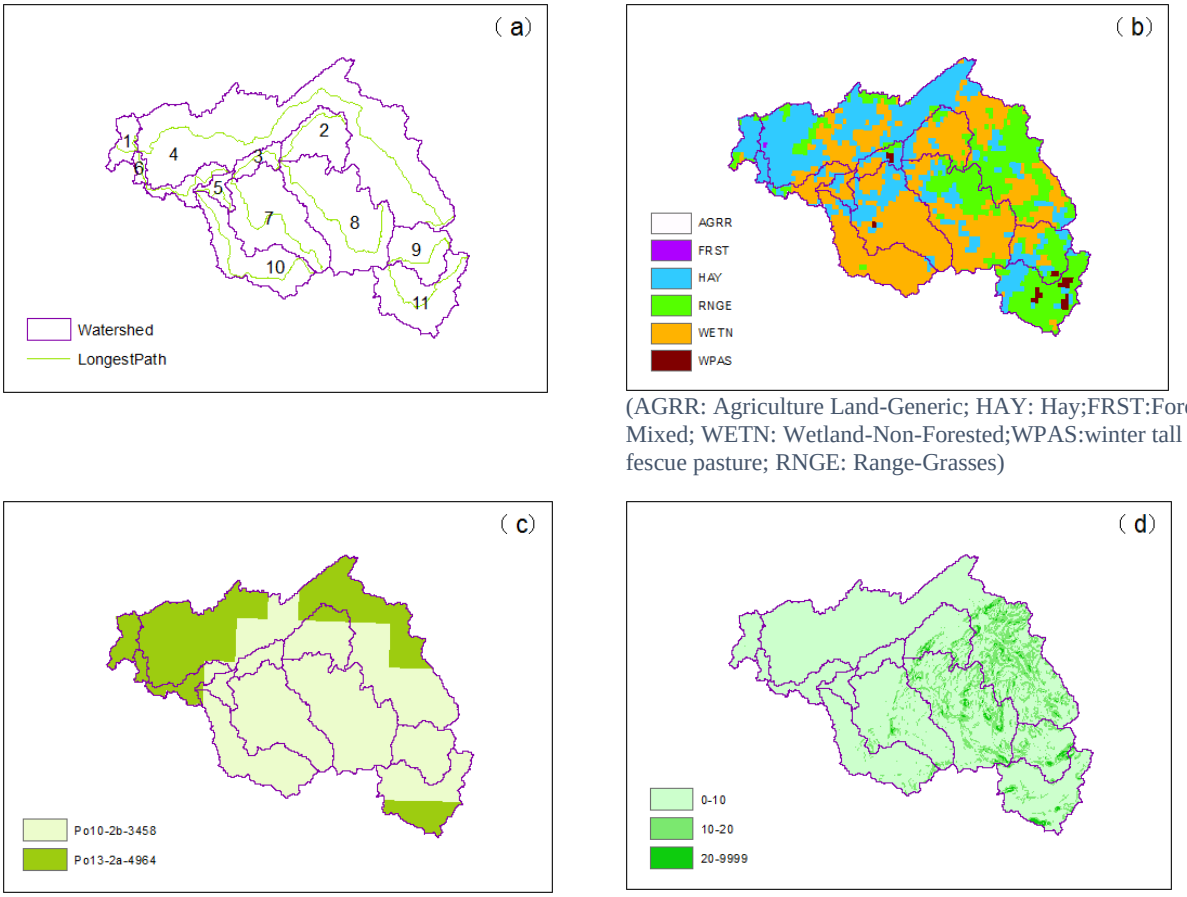

(AGRR: Agriculture Land-Generic; HAY: Hay;FRST:Forest-Mixed; WETN: Wetland-Non-Forested;WPAS:winter tall fescue pasture; RNGE: Range-Grasses)

(Po10-2b-3458: loam; Po13-2a-4964: loam)

Figure 3-4: Maps of the Nicolet River watershed. (a) delineated subwatershed, (b) landuse, (c) soil type, and (d) slope.

3.3.3.2 Meteorological and Hydrological Data

Meteorological data, including the daily maximum temperature, minimum temperature and precipitation was obtained from Environment Canada. Four weather stations (Climate ID:701HE63; 7027783; 7022160; 7027248) located inside or around the catchment were employed. Daily air temperature data and precipitation data collected from 1983 to 2000 were used as data inputs for the model. The datasets were split into three periods: model warm-up (1983-1985), model calibration (1986-1990), model validation (1991-2000).

Table 3-2: Location of weather stations

Station Name	Station ID	Longitude	Latitude
TROIS RIVIERES AQUEDUC	701HE63	72°62' W	46°38' N
ST WENCESLAS	7027783	72°33' W	46°17' N
DRUMMONDVILLE	7022160	72°48' W	45°88' N
ST FERDINAND	7027248	71°58' W	46°10' N

The historical stream flow data from the Bulstrode River (ID: 02OD003), 5.8 km from the main stream of the Nicolet River was available in the HYDAT database of Environment Canada. Monthly streamflow from 1983 to 2000 showed a seasonal pattern where spring flow affected by snowmelt represented most of the annual runoff volume, followed by secondary high flow events in the late summer or autumn (Figure 3-5). The discharge declines gradually from late autumn to winter, then reaches a minimum value in early spring.

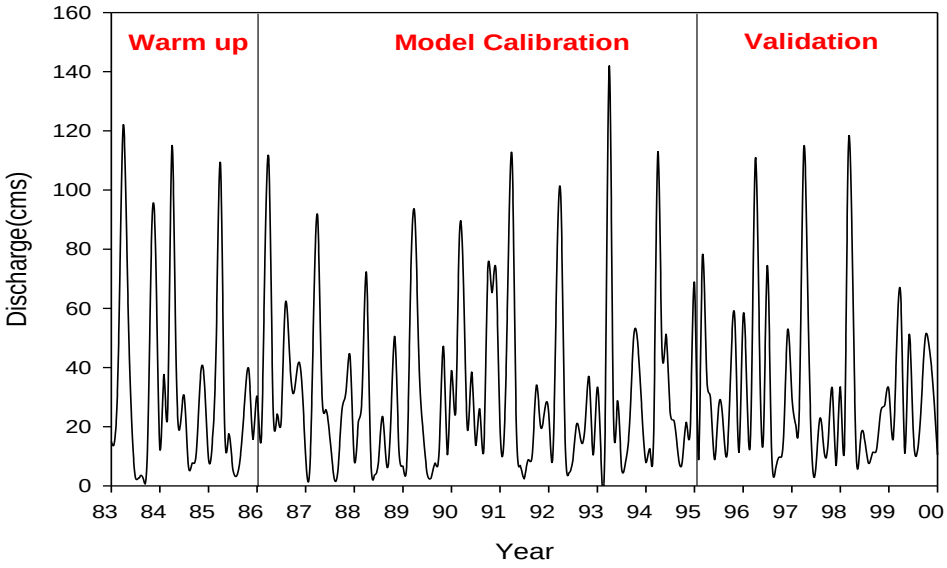

Figure 3-5: Observed monthly streamflow for 1983-2000 for study area

3.3.4 Model Calibration and Validation

The model was initialized with 1983-1985 data and was then run on both daily and monthly time steps for the period of 1986-2000. Five-years outputs from 1986 to 1990 were used for model calibration and ten-years outputs from 1991 to 2000 were used for model validation. Once the model was successfully running, SWAT Check was executed for default output to examine the availability of water in each hydrological component, *i.e.*, the water equivalent of precipitation, evapotranspiration, groundwater, surface runoff, soil water content and water yield. Water balance equations are employed to assess the rationality of model output and provide a guide for calibrating the model. The water balance error (ERR_{wb}) over a given timestep was calculated as:

$$\mathrm{ERR_{wb}} = \mathrm{PRECIP} - (\mathrm{WYLD} + \mathrm{ET} + \Delta\theta + \mathrm{Deep\ Seepage}) \quad 3\text{-}13$$

where,

$$\mathrm{WYLD} = \mathrm{SURQ} + \mathrm{LATQ} + \mathrm{GW_Q} - \mathrm{TLOSS} - \mathrm{pond\ abstractions} \quad 3\text{-}14$$

where,

$\mathrm{GW_Q}$ is the groundwater contribution to streamflow (mm),

LATQ	is the lateral flow contribution to streamflow (mm),
PRECIP	is the total precipitation (mm),
SURQ	is the surface runoff contribution to streamflow (mm),
TLOSS	are transmission losses from tributary channels (mm),
WYLD	is the total water yield (mm H_2O), and
$\Delta\theta$	is the change in soil water content (mm).

Sensitivity analysis is the first step in calibrating the model, allowing one to identify key parameters and their ranges of sensitivity. A full description of parameters can be obtained in the SWAT theoretical documentation (Neitsch et al., 2011). A local sensitivity analysis method was adopted, which allows single parameters to be individually changed gradually from a maximum to a minimum value (Arnold et al., 2012b). The range chosen for a given sensitivity test differed from the maximum range given by SWAT; for example, considering the study watershed's range of land use, hydrologic conditions, and hydrologic soil groups, the parameter CN2 was tested from 74 to 86 instead of the maximum range of 35 to 98 with. Sensitivities are defined by the percentage change in water yield, surface runoff, and subsurface flow with respect to specific percent changes in the parameters subjected to sensitivity analysis. This analysis completed, the most sensitive parameters are adjusted until the optimal model accuracy is achieved.

Overall, three common problems were detected by the default model performance:

(i) The streamflow was generally overestimated in summer, and underestimated in winter, especially with respect to peak discharges;

(ii) the hydrography of simulated results was consistently a few days ahead of observations;

(iii) several small winter discharges were missed by the simulation and replaced by a primary peak value.

Accordingly, the objectives of the calibration were to:

(i) increase surface runoff, while decreasing summer stream flow by increasing ET;

(ii) shorten the time of concentration;

(iii) control the snow-related parameters to better simulate early spring peak flows.

Among all parameters, those influencing the whole period are firstly selected to correct the problems with the timing and volume of discharge, and get a reasonable result for water yield, surface runoff, and subsurface runoff. Then, snowmelt-related parameters are optimized to yield a better performance in winter. For the validation phase, all the parameters remained unchanged.

3.3.5 Assessment of Model Performance

Moriasi et al. (2007) assessed various accuracy evaluation methods for hydrological models and established guidelines based on the previous studies. The Nash-Sutcliffe efficiency (NSE), RMSE-observations standard deviation ratio (RSR) and Percent Bias (PBIAS) were adopted in this study to evaluate the performance of ArcSWAT in modelling streamflow in the Nicolet River watershed. With a range of $-\infty < \mathrm{NSE} \leq 1$, NSE = 1.0 indicates a perfect agreement between simulation and observation, while $\mathrm{NSE} \leq 0$ indicates that the observed mean is an equally or more accurate predictor than the simulated result. Values of NSE > 0.5, $0.65 \leq \mathrm{NSE} \leq 0.75$, and NSE > 0.75 indicate satisfactory, good, and very good model performance (Moriasi et al., 2007). The value of the NSE as given as (Nash and Sutcliffe, 1970):

$$\mathrm{NSE} = 1 - \left[\frac{\sum_{i=1}^{i=n}\left(Y_i^{obs} - Y_i^{sim}\right)^2}{\sum_{i=1}^{i=n}\left(Y_i^{obs} - \overline{Y^{obs}}\right)^2}\right] \qquad 3\text{-}15$$

where,

n is the number of observed or simulated values,

Y_i^{obs} is the i^{th} observed value,

$\overline{Y^{obs}}$ is the mean of observed values, and

Y_i^{sim} is the i^{th} observed value.

The RSR is deemed acceptable if RSR < 0.7 (Singh et al., 2005):

$$\mathrm{RSR} = \frac{\sqrt{\sum_{i=1}^{n}\left(Y_i^{obs} - Y_i^{sim}\right)^2}}{\sqrt{\sum_{i=1}^{n}\left(Y_i^{obs} - \overline{Y^{obs}}\right)^2}} \quad 3\text{-}16$$

The optimal value of PBIAS is 0, positive and negative values indicating model underestimated bias and overestimated bias, respectively (Maréchal, 2004). A model is deemed to provide an acceptable accuracy when $|PBIAS| \leq 15\%$.

$$\mathrm{PBIAS} = 100 \cdot \frac{\sum_{i=1}^{n}(Y_i^{obs} - Y_i^{sim})}{\sum_{i=1}^{n} Y_i^{obs}} \quad 3\text{-}17$$

3.4 Results and Discussion

3.4.1 Model Calibration

3.4.1.1 Sensitivity Analysis

The soil evaporation compensation factor (ESCO), which influences the water yield by controlling the amount of water in the soil layers available for soil evaporation, is the most sensitive parameter with respect to simulating water yield (Table 3-3). The CN2 parameter was the most sensitive parameter with respect to surface runoff, but it had little effect on water yield, making it a good parameter to partition precipitation into infiltration and runoff. Slope length for lateral subsurface flow (SLSOIL), which decides subsurface flow velocity, notably influenced subsurface flow. The groundwater "revap" coefficient, controlling water movement from the shallow aquifer to the root zone, and available water capacity of the soil layer (SOL_AWC) also played an important role in determining subsurface flows, as well as water yield.

Table 3-3: Results of sensitivity analysis

Parameter	Sensitivity Rank			Range		Water yield (mm)		Surface Flow (mm)		Subsurface Flow (mm)	
	WY	SF	SSF	Min	Max	Min	Max	Min	Max	Min	Max
CN2	-	1	4	74	86	499.76	500.81	154.12	284.09	204.85	326.72
GW_REVAP	3	-	3	0.02	0.2	377.02	499.76	212.07	212.07	149.48	272.22
ESCO	1	3	5	0.01	1	391.43	561.89	197.62	213.49	183.07	287.15
SLSOIL	4	2	1	0	150	371.55	425.45	167.87	212.32	0	272.22
SOL_AWC	2	-	2	0	1	354.39	489.79	208.46	214.49	213.29	337.71

Note: CN2 is initial SCS runoff curve number for moisture condition II, GW_REVAP is groundwater "revap" coefficient, ESCO is soil evaporation compensation factor, SLSOIL is slope length for lateral subsurface flow, SOL_AWC is available soil water content.

3.4.1.2 Calibration

Given the soil type and land use in the study area, the watershed was characterized as having slow infiltration and water transmission rates, along with a high runoff potential. The parameters initially adjusted to match simulated streamflow to observed streamflow were GW_REVAP, SOL_AWC, SLSUBBSN, ESCO, along with CN2. While the range of CN2 suggested by the handbook (Arnold et al., 2012a) is from 74 to 86, a slightly bias in the range employed is acceptable because of residual soil moisture from previous precipitation (Gombault et al., 2015). The optimal values for the different HRUs modelled exceeded default values by 11%, which falls within the acceptable range for the PBIAS. Serving to decide the depth of soil used to meet the soil evaporative demand, the ESCO parameter was calibrated from a default value 0.95 to 0.65 to allow the model to extract more water for evaporation from lower layers, thereby increasing summer ET. The value of GW_REVAP was increased from 0.02 to 0.05, allowing more water transfer from the shallow aquifer to the root zone. Although model outputs were sensitive to SOL_AWC and SLSOIL, these variables' default values were identified as the optimal values. In addition to the most sensitive parameters, GW_DELAY and ALPHA_BF were modified to

achieve a better simulation. For this study, the value of ALPHA_BF was increased from a default value of 0.048 to 0.5 to decrease summer baseflow. Representing the time that water takes to infiltrate through the soil layers and reach the shallow aquifer, the value of groundwater delay time (GW_DELAY) was adjusted from a default value of 31 days to a value of 80 days, to address the model's slow rate of water transmission and infiltration.

While the sensitive parameters can control the amount of the water available for each component, the streamflow can be further controlled through the average slope length (SLSUBBSN), average slope steepness (SLOPE), and Manning's "n" value for the tributary channels (CH_N1). Accordingly, SLSUBBSN was increased by 10% compared with the default value, SLOPE was decreased by 20% to shorten the time of concentration, and — based on model handbook recommendations for the land with moderate vegetative cover (Arnold et al., 2012a) — Manning's "*n*" value for the tributary channels was increased from 0.014 to 0.05.

In the study area, peak discharge over a single year was strongly influenced by snowmelt, but difficult to simulate given the complexity of snowmelt process and its energy interactions. Based on the sensitivity analysis, four of seven snowmelt-related parameters (i.e., SFTMP, SMTMP, SMFMX, and SMFMN) were shown to provide the greatest sensitivity with respect to the tweaking the snowmelt process. An optimal value of SFTMP of -1°C, resulted in an increase of the volume of snowfall, as well as a later snowmelt. In winter, the shape and peaks of the hydrograph were mainly controlled by SMTMP, the snowmelt base temperature above which snowpack melts. Accordingly, an increase of SMTMP from 0.5°C to 3.5°C yielded a better simulation of streamflow, decreasing the volume of winter peaks, and dividing major peaks into several sub-peaks. The impact of snowpack density on snow melt was represented by the maximum and minimum snowmelt rates (SMFMX and SMFMN, respectively), with values ranging from 1.4 to 6.9 mm d^{-}

^{1} °C^{-1} in rural areas, and 3.0 to 8.0 mm d^{-1} °C^{-1} in urban areas. The calibrated values of SMFMX and SMFMN were 5℃ and 5.5℃, respectively, indicating relatively large seasonal variations in this model. In addition, the parameter of minimum snow water content that corresponds to 100% snow cover (SNOCOVMX) was increased from 1 to 50, such that the areal depletion curve assumed a greater important in the snow melt process. Similarly, SNO50COV was adjusted to 0.2 to obtain a better simulation in winter.

Finally, the model performed in a satisfactory manner for daily flow (NSE=0.51, RSR=0.69, and PBIAS=-5.54%) and a good to very good manner for monthly stream flow (NSE=0.84, RSR=0.49, and PBIAS: -5.57%. The water balance error for the calibration period was 5%.

Table 3-4: Summary of the calibrated parameters: definition, unit, default value, range and optimal value

Parameters	Definition	Unit	default value	optimal value
CN2	Initial SCS runoff curve number for moisture condition II	-	-	+11%
GW_REVAP	Groundwater "revap" coefficient	-	0.02	0.05
ALPHA_BF	Baseflow alpha factor	days	0.048	0.5
GW_DELAY	Groundwater delay time	days	31	80
ESCO	Soil evaporation compensation factor	-	0.95	0.65
CH_N1	Manning's "n" value for the tributary channels	-	0.014	0.05
SURLAG	Surface runoff lag coefficient	-	2	1.3
SLOPE	Average slope steepness	m m^{-1}	-	-20%
SLSUBBSN	Average slope length	m	-	10%
SFTMP	Snowfall temperature		1	-1
SMTMP	Snow melt base temperature		0.5	3.5
SMFMX	Melt factor for snow on June 21		4.5	5
SMFMN	Melt factor for snow on December 21		4.5	5.5
SNOCOVMX	Minimum snow water content that corresponds to 100% snow cover	mm	1	50
SNO50COV	Fraction of snow volume represented by SNOCOVMX that corresponds to 50% snow cover	-	0.5	0.2

3.4.2 Model Validation

The model was validated over the period of 1996-2000 on both daily and monthly time steps. The ArcSWAT model showed a good performance in simulating monthly streamflow and a satisfactory performance simulating daily streamflow (Table 3-4). The model had an acceptable performance in simulating spring stream flows which were predominantly attributable to snowmelt. Overall, the model was capable to accurately simulate the timing of peak flows, but, the volume of peak flows was slightly underestimated. For the monthly step, the NSE value is 0.77, the RSR value is 0.48 and the PBIAS value is 2.04. For the daily step, the NSE value is 0.51, the RSR value is 0.69 and the PBIAS value is 2.13. Overall, the validation of the model developed for the Nicolet River showed that the ArcSWAT model could represent the watershed's physical and hydrological characteristics in an adequate manner.

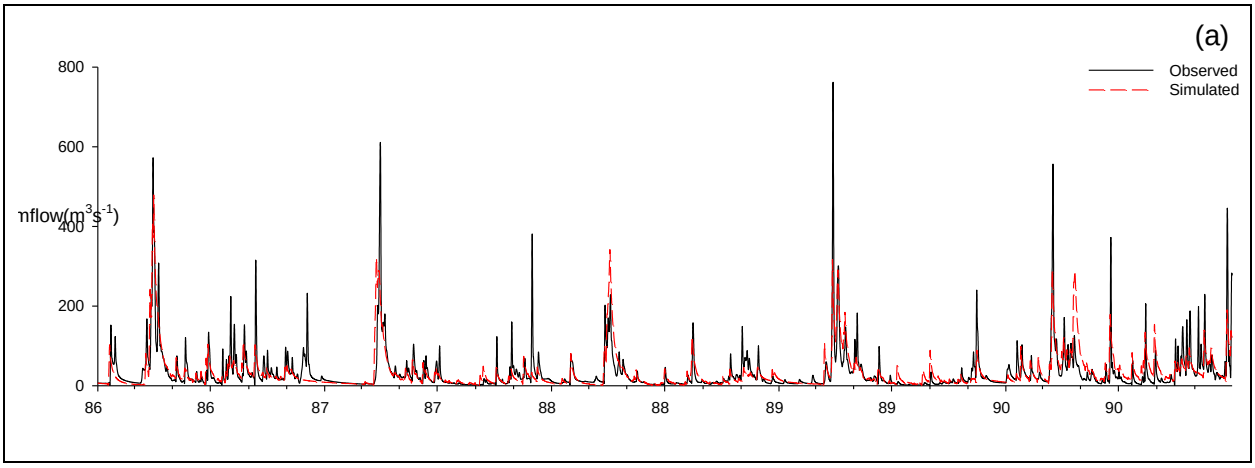

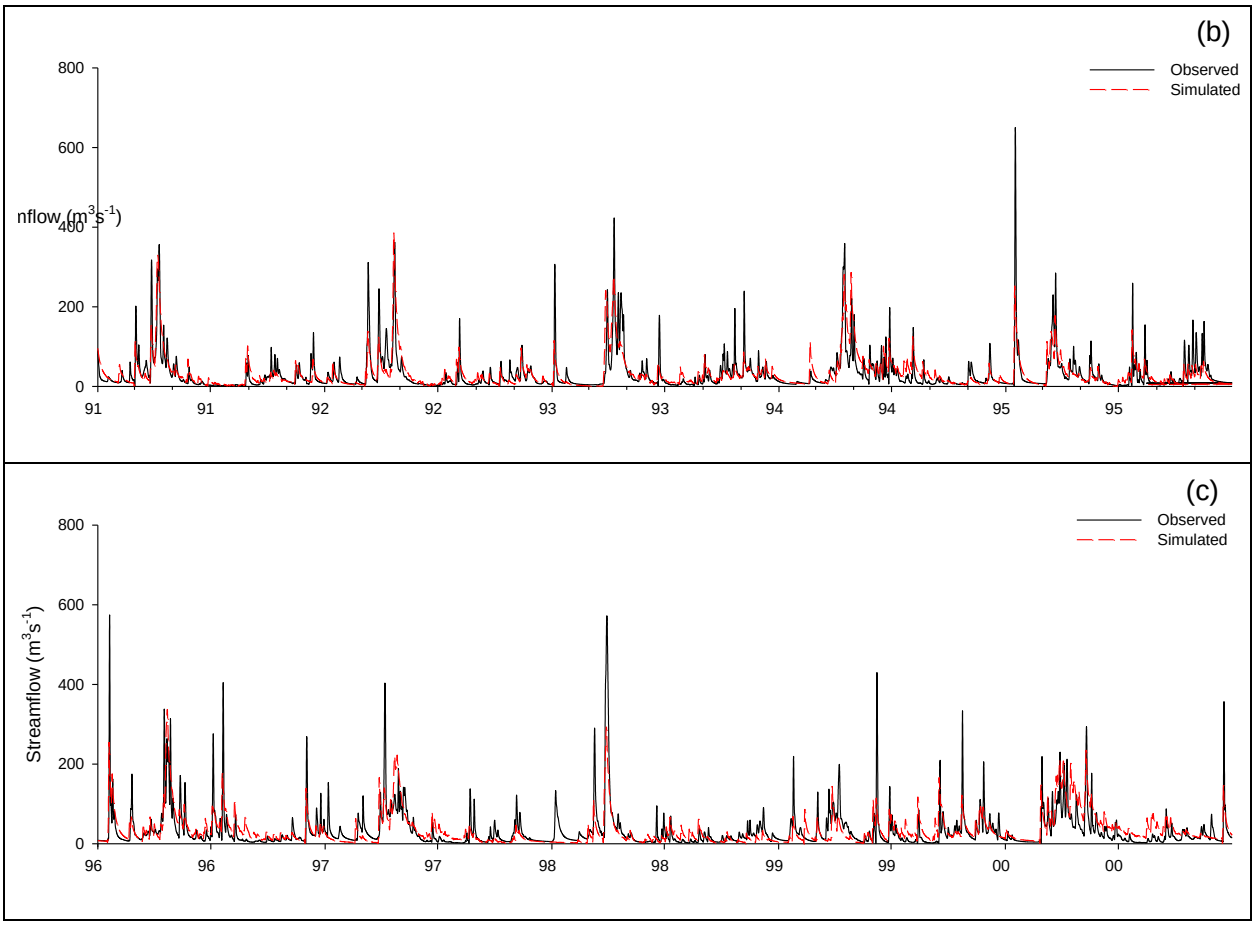

Figure 2-6: Observed and simulated streamflow in the Nicolet River watershed: (a) calibrated phase, 1986-1990; (b,c) validated phase, 1991-2000.

Table 3-4: Statistics of calibrated and validated results for yearly and daily streamflow

Modelling phase	Time step	Statistics		
		NSE	RSR	PBIAS
Calibration (1986-1990)	Daily	0.55	0.67	8.97
	Monthly	0.75	0.50	8.72
Validation (1991-2000)	Daily	0.51	0.69	2.13
	Monthly	0.77	0.48	2.04

3.4.3 Discussion and Conclusions

As discussed before, the streamflow pattern in Nicolet river is characterized by two large streamflow events: a primary peak flow in spring, followed by a secondary peak flow in summer or fall. The simulated streamflow strictly followed the observed streamflow pattern. Over the 1986-2000 period, a large amount of streamflow occurred in late winter and early spring moths,

coinciding with the snowmelt seasons. However, the months of late summer and autumn had secondary peak flows, which resulted from large rainfall events.

The ArcSWAT model's capacity to simulate the hydrology of the Nicolet River watershed was confirmed. The parameter sensitivity tests undertaken in the model's calibration phase (1986-1990 data) showed model outputs to be sensitive to CN2, GW_REVAP, ESCO, SLSOIL, and SOL_AWC. It was important to accurately simulate both the volume and timing of peak flow events. Given that, in the watershed under study, peak flows were predominantly affected by snowmelt, and sensitive to SFTMP, SMTMP, SMFMX, and SMFMN values. The value of SFTMP influences the quantity of snow accumulation, with a lower value of SFTMP resulting in an increased snowfall. As SMTMP was most sensitive parameter influencing the magnitude and occurrence of peak flow events, its decrease resulted in reduced simulated winter peak flows. Both SMFMX and SMFMN influenced the magnitude of each snowmelt event, and therefore the volume of peak flow arising from these events. After calibration, the model yielded a satisfactory performance in simulating daily streamflow (NSE = 0.55, RSR = 0.67 and PBIAS = 8.97%). The water balance error during the calibration period was 3%. The model was validated over the period of 1991-2000, yielding a tool which also simulated daily Nicolet River streamflow reasonably well (NSE = 0.51, RSR = 0.69 and PBIAS of 2.13%).

Given that the quality of input data decides the accuracy of streamflow simulation, the greatest challenge which arose during this study was data acquisition. Further work can therefore focus on the data collection. Accordingly, the following recommendation are made:

i) Continued gathering of long-term meteorological information, including precipitation, temperature, wind, and solar radiation for the Nicolet River to provide a more accurate and diverse dataset for data input;

ii) Continued monitoring of streamflow at the watershed's outlet to provide longer term streamflow observations. This could significant strengthen the accuracy of ArcSWAT simulations for this watershed.

Chapter 4 Impacts of Climate Change on the Hydrologic Cycle in the Nicolet River Watershed

4.1 Abstract

The impacts of climate change on streamflow in the Nicolet River watershed (Quebec, Canada), particularly those on snowfall, snowmelt, and peak flow, were assessed using a version of the ArcSWAT model calibrated and validated to historic watershed streamflow and supplied with future climatic data drawn from 11 pairs of regional climate models (RCMs) and global climate models (GCMs) provided by the North American Regional Climate Change Assessment Program (NARCCAP). Besides focusing on the impact of climate change on peak flow, the present study assessed the individual rather than combined effects of temperature and precipitation on snowfall and snowmelt. Analysis of data generated by different climate change scenarios showed that annual mean temperature was projected to increase by 2°C—3.1°C, and annual precipitation by 12%—34% between the baseline period of 1983-2000 and the projected period of 2038-2068. The largest and smallest increases occurred in the winter and summer, respectively. On average, model simulations predicted a 30% increased in mean annual streamflow, with the greatest increase occurring in the winter, a moderate increase in summer and fall, and a slight decrease in spring. Peak flow was predicted to increase by 13% relative to the baseline period, and earlier peak flow is forecasted under all of the future climate scenarios. The separated effects of temperature and precipitation on streamflow reveal that while the increase of peak flow is dominated by increased precipitation, the timing of peak flow occurrence is mostly affected by the temperature.

4.2 Introduction

Altered trends in climatic variables (e.g., precipitation, temperature, etc.) arising from climate change may contribute to the intensification of the hydrological cycle (Huntington, 2006). Over

the 20th century, annual mean temperatures in southern Canada have risen by 0.5°C to 1.5°C, while annual precipitation has risen by 5% to 35% (Zhang et al., 2000). Similarly, over the period of 1960 to 2005, annual mean temperatures in southern Quebec have risen between 0.6°C and 1.8°C, while total annual precipitation for the region has risen by 20 mm y^{-1} to 100 mm y^{-1} (Yagouti et al., 2008). The most significant warming occurred in winter and summer. According to the Fifth Assessment Report (AR5) of International Panel on Climate Change (IPCC), global mean temperature will continue to increase by 0.3°C-4.8°C for the period of 2046-2065 when compared to 1986–2005 base period depending on different assumptions of the concentration-derived RCPs (IPCC, 2013). Shifts in precipitation and temperature are critical to the hydrology of watersheds. In Quebec, high flow events and spring floods were particularly affected by snowmelt, which accounted for up to 40% of annual streamflow (Coulibaly et al., 2000; Ferguson, 1999). With rising winter temperatures, more precipitation may fall as rain, leading to the reduction of snow accumulation and an increase in ice density. Higher winter temperatures may also result in an earlier onset of snowmelt and a shorter period of frost days (Mortsch et al., 1999; Stewart, 2009). While an alteration in temperature would particularly affect the timing of snowmelt, changes in precipitation could influence the volume of the snow cover and associated snowmelt(Barnett et al., 2005). The several previous studies which used SWAT to simulate the hydrological response of southern Quebec watersheds to climate change, showed that higher total runoff, along with earlier snowmelt and discharge peaks could be expected (Gombault et al., 2015; Minville et al., 2008; Shrestha et al., 2012). While none of these studies addressed stream flow or peak flow in the Nicolet river, the potential impacts of climate change on the nearby Pike River watershed was studied by Gombault et al. (2015). They found that, compared to the baseline period of 1971-2000, annual streamflow would increase by 9-19% under the future scenarios (2041-2070), and more

notably, that winter streamflow would increase 2- to 3-fold. As the four future climate models, developed through different assumptions, showed a large variation in projections in terms of spatial and seasonal changes, it became essential to apply multiple climate change models to assess the full possible range of climate change impacts within the Nicolet River watershed. Previous studies primarily focused on how the combined effects of temperature and precipitation affected peak flow (Gombault et al., 2015; Minville et al., 2008; Shrestha et al., 2012); however, for a snow-dominated watershed, where peak flow is mainly influenced by snowmelt, it is important to discriminate between the effects of changes in temperature and changes in precipitation on snowfall and snowmelt.

While global climate change has attracted widespread attention to increased greenhouse gas emissions, specific regional climate-induced discrepancies have highlighted the need for finer resolution of climate change scenarios. Generally, a downscaling approach has been used to improve the coarsely gridded data of global climate models (GCMs) for their application in watershed-level hydrological areas. The North American Regional Climate Change Assessment Program (NARCCAP) is a major international program which applies the downscaling approach to global climate models (GCMs) by embedding the regional climate models (RCMs) for North America. The RCMs are nested within GCMs for both the current period and future periods so as to be able to generate climate data for the current period and future periods.

The main objective of this chapter is to quantify the potential effects of climate change on the hydrology of the Nicolet River watershed. This research focuses on hydrologic changes induced by climate change between the baseline period (1986-2000) and a projected future climate (2053-2067), especially in the winter and spring seasons. The ArcSWAT model was calibrated and validated for the baseline period (1986-2000) in Chapter 3. The model showed good accuracy in

both the calibration phase (NSE = 0.75 for monthly time step and NSE = 0.55 for a daily time step) and validation phase (NSE = 0.77 for monthly time step and NSE = 0.51 for a daily time step). Projected current climate data and future climate data were provided by NARCCAP but were not introduced directly into the ArcSWAT model because the projected current climate scenario was not always representative of the current situation.

The characteristics of Nicolet River watershed have been outlined in Chapter 3. In this chapter, the source of climate scenarios and bias correction methods, as well as a brief description of model calibration and validation, will be presented (Section 3). Climate variability and changes of 11 climate scenarios will then be analysed. Finally, the simulated impact of climate change on the Nicolet River watershed's hydrology will be assessed using the both calibrated and validated ArcSWAT model (Section 4).

4.3 Material and Methods

4.3.1 Climate Scenarios

The future climate was acquired from the North American Regional Climate Change Assessment Program (NARCCAP), which is an international program providing high solution climate change scenarios for North America. Regional climate models (RCMs) were embedded into a coupled General Circulation Model (GCMs) to obtain regional climate data. The eleven RCM-GCM pairings investigated (Table 4-1) generated eleven current climate projections (1971-1998) and a further 11 future climate projections (2038-2068). Historical observations from 1983-2000 provided by Environment Canada served to generate the baseline output. Four meteorological stations (Climate ID:701HE63; 7027783; 7022160; 7027248) were used to provide the climate input data.

Table 4-1: RCM-GCM combinations used for generating meteorological data

		GCM			
		GFDL	CGCM3	HadCM3	CCSM
RCM	CRCM		*		*
	MM5I			*	*
	HRM3			*	
	RCM3	*	*		
	ECP2	*		*	
	WRFG		*		*

4.3.2 Climate data and Bias Correction

As projected future climate data is generated based on projected current climate data, which may not always be representative of current climate conditions, the future climatic data cannot be used directly for climate change research. Accordingly, the change factor (CF) method was employed to correct the bias between projected and observed climate data (Chen et al., 2011; Minville et al., 2008). In the CF method, future climate data are created by superimposing the monthly differences between projected future climate data and projected current climate data onto historical observations. To obtain the differences, we generated historical (1983-2000) and future (2050-2067) daily climate data for four weather stations using all of 11 climate scenarios. With these two data sets, 67 years apart, monthly differences between historical and future data were calculated. Changes in weather variables were generated by subtracting the monthly average of projected historical weather data from the monthly average of projected future weather data. Then for each climate scenario, the changes in temperature (in ℃) and precipitation (in %) were added to historical daily maximum and minimum temperature data and daily precipitation data respectively. Future climate input generated by the CF method for temperature and precipitation are given as:

$$T_{adj,future,d} = T_{obs,d} + (\overline{T}_{RCM,future,m} - \overline{T}_{RCM,baseline,m}) \quad 4\text{-}1$$

$$P_{adj,future,d} = P_{obs,d} \cdot \frac{\overline{P}_{RCM,future,m}}{\overline{P}_{RCM,baseline,m}} \quad 4\text{-}2$$

where,

$P_{adj,future,d}$ future daily precipitation data adjusted by the change factor method,

$P_{obs,d}$ observed daily data of baseline period for temperature and precipitation

$\overline{P}_{RCM,baseline,m}$ monthly average precipitation data for the baseline period for each regional climate model

$\overline{P}_{RCM,future,m}$ monthly average precipitation data for future period for each regional climate model

$T_{adj,future,d}$ future daily temperature data adjusted by the change factor method,

$T_{obs,d}$ are observed daily data of baseline period for temperature and precipitation, respectively,

$\overline{T}_{RCM,baseline,m}$ monthly average temperature data for baseline period for each regional climate model,

$\overline{T}_{RCM,future,m}$ monthly average temperature data for future period for each regional climate model.

4.3.3 Model Validation and Application

The ArcSWAT model, used the present climate change study targeting the Nicolet River watershed, was calibrated for 1986-1990 and validated for 1991-2000. The optimal parameter values were selected for climate change simulation based on statistical criteria. The model yielded good results for streamflow: NSE = 0.75, 0.77, 0.55, and 0.51 for monthly estimates in in calibration and validation phases, and daily estimates in calibration and validation phases, respectfully. The adjusted future climate projections during 2050-2067 were derived from the same weather stations as the baseline data (Climate ID:701HE63; 7027783; 7022160; 7027248), as these were used for model calibration and validation. While the first three years (2050-2052) were used

to warm up the model, the model ran on daily time step for 2053-2067 for each climate scenario, with corresponding daily and monthly results obtained for each of the climate scenarios.

4.4 Results and Discussion

4.4.1 Climate Variability and Change

Analysis of annual and seasonal changes were conducted for precipitation and temperature. Averaging across 11 climate scenarios, mean annual temperature were projected to increase by 2.6℃ compared with the baseline value of 4.2 ℃. All scenarios show temperature increases for the Nicolet River during the period of 2053-2067, with the magnitude of increase ranging from 2.0℃ to 3.1 ℃. Mean annual precipitation is forecasted to increase from a baseline value 1230 mm to 1488 mm (+21%) when averaging all scenarios. The increase in precipitation occurred for all scenarios and varied from 12% to 34%.

Hydrological responses to climate change at a watershed scale are closely related to seasonal climate change. Mean seasonal temperatures rose by 2.1℃ (range 1.5℃-2.8 ℃), 2.2 ℃ (range 1.6℃-2.9 ℃), 2.5℃ (range 2.1℃-3.0 ℃) and 3.2℃ (range 2.4℃-4.1℃) for spring (March-May), summer (June-August), autumn (September-November), and winter (December-February), respectively (Table 4-2). The large increase in winter and spring temperature could reduce the amount of snow accumulation and snowmelt, thus affecting streamflow. For precipitation, all scenarios showed an increase is illustrated by. Seasonally, the precipitation increases 20% (range 6%-35%),18% (range 8%-42%), 21% (range 3%-42%) and 27% (range 16%-52% in spring, summer, autumn and winter, respectively. As these changes indicate that future peak flows may be affected by a combination of rainfall and snowmelt, the complexity of their analysis is increased. Moreover, the large inter-model variability may be the result of the large variance in hydrologic response.

Table 4-2: Seasonal and Annual weather variables for future climate scenarios (2053-2067), and for baseline period 1986-2000

Climate Scenarios	Mean seasonal temperature (℃)					Mean seasonal precipitation(mm)				
	Spring	Summer	Autumn	Winter	Annual	Spring	Summer	Autumn	Winter	Annual
Baseline	6.0	3.4	17.1	-9.9	4.2	262.8	362.8	307.0	297.0	1229.6
CRCM_CCSM	8.0	5.7	19.8	-6.2	6.8	292.9	391.4	346.4	372.9	1407.0
CRCM_CGCM3	8.8	6.1	19.4	-7.3	6.8	325.0	395.6	353.4	408.0	1491.5
ECP2_GFDL	8.6	5.2	19.6	-5.8	6.9	326.1	430.9	357.7	441.1	1561.2
ECP2_HadCM3	7.9	5.2	20.0	-6.2	6.7	321.6	516.1	435.6	414.7	1678.9
HRM3_GFDL	8.6	6.3	19.9	-6.3	7.1	294.1	336.9	336.7	385.0	1365.1
HRM3_HadCM3	8.2	6.3	20.1	-7.1	6.9	309.3	417.7	401.7	392.5	1524.2
MM5I_CCSM	7.8	5.1	19.6	-6.7	6.4	288.7	474.7	400.2	375.9	1529.8
MM5I_HadCM3	8.6	5.6	19.8	-5.9	7.0	316.2	414.7	359.7	358.8	1452.8
RCM3_CGCM3	8.5	6.1	19.5	-6.8	6.8	353.5	440.2	378.8	346.1	1524.0
RCM3_GFDL	7.8	6.1	19.4	-7.5	6.4	327.6	397.2	340.3	351.9	1424.7
WRFG_CCSM	7.9	5.0	19.9	-6.3	6.6	277.8	429.0	316.0	359.0	1376.5
WRFG_CGCM3	7.5	5.1	19.2	-7.5	6.1	339.9	415.6	381.4	368.9	1513.5

4.4.2 Hydrological impacts of climate change

4.4.2.1 Mean annual and seasonal flows

A comparison of annual and seasonal streamflow between baseline (1983-2000) and future scenarios (2053-2067) show a future increase in mean annual streamflow, which averaged 30% across all projections (Table 4-3). The large inter-model variation is demonstrated by all the simulations. The largest (47.2%) increase in mean annual streamflow is produced by the ECP2_HadCM3 projection, and the smallest variance (8%) by the WRFG_CCSM projection. For the predicted increases in annual streamflow coincided with a corresponding increase in mean annual precipitation; specifically, higher overall precipitation is responsible for greater streamflow at an annual scale.

All projections suggested increases in summer, autumn, and winter discharge; however, there was no consensus on spring stream flow among the different climate scenarios. While the

simulations of CRCM_CCSM, ECP2_HadCM3, HRM3_HadCM3, MM5I_HadCM3, RCM3_CGCM3 and WRFG_CCSM suggested a decrease in spring streamflow, the remaining projections suggested an increase in spring streamflow. When averaging all the future climate scenarios, the spring streamflow decreased by 1.1 $m^3 s^{-1}$ compared with the baseline period. The largest increase happened in winter with an average increase of 80% against the baseline period, whereas more moderate increases (30%) occurred in summer and autumn.

Table 4-3: Seasonal and annual streamflow for future climate scenarios (2053-2067), and for baseline period 1986-2000

Climate Scenarios	Streamflow ($m^3 s^{-1}$)				
	Spring	Summer	Autumn	Winter	Annual
Baseline	59.2	24.1	20.8	23.5	31.9
CRCM_CCSM	56.8	27.5	23.5	37.1	36.2
CRCM_CGCM3	61.6	27.5	23.7	42.4	38.8
ECP2_GFDL	60.6	33.6	25.4	51.8	42.9
ECP2_HadCM3	55.7	44.3	38.3	49.4	46.9
HRM3_HadCM3	56.2	28.8	30.6	42.3	39.5
MM5I_CCSM	60.8	41.6	37.3	44.9	46.1
MM5I_HadCM3	49.0	29.3	25.0	39.9	35.8
RCM3_CGCM3	57.7	33.3	27.8	40.1	39.7
RCM3_GFDL	61.9	28.0	23.5	35.8	37.3
WRFG_CCSM	51.2	31.1	19.7	36.9	34.7
WRFG_CGCM3	67.1	31.4	29.8	37.6	41.5

4.4.2.2 Peak Flows

Annual peak flows projected under the different climate scenarios were analysed according to the magnitude of peak flow (Figure 4.1) and its timing (Table 4-4). In terms of the volume of peak flow, CRCM_CCSM, MM5I_HadCM3, RCM3_CGCM3, and WRFG_CCSM suggest slight decreases (median value) in peak flows, whereas the remaining of scenarios propose increases (median value) ranging from 6% to 36%. On average, the volume of peak flow was increased by 13% compared to the baseline period. In terms of the timing of peak discharge,

Table 4-4 indicates that all the simulations suggest an earlier peak. During the baseline period most peak flow events happened in March and April, whereas under future scenarios the number of peak flow events in March is predicted to increase, and that in April to decrease.

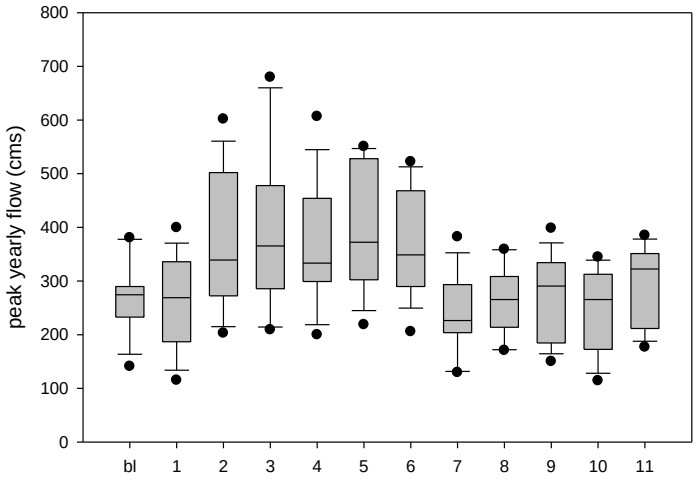

Figure 4-1: Peak yearly discharges for all scenarios for 2053-2067, and for baseline period 1986-2000 (Explanation of the x-axis legends: bl: baseline; 1:CRCM_CCSM; 2:CRCM_CGCM3; 3:ECP2_GFDL; 4:ECP2_HadCM3; 5:HRM3_HadCM3; 6:MM5I_CCSM; 7:MM5I_HadCM3; 8:RCM_CGCM3; 9:RCM3_GFDL; 10:WRFG_CCSM; 11:WRFG_CGCM3)

Table 4-4: The time of occurrences of peak flow for each month for all scenarios for 2053-2067, and for baseline period 1986-2000

	Jan	Feb	Mar	Apr	May	Aug	Sep	Nov	Dec
Baseline	2	-	4	6	2	-	1	-	-
CRCM_CCSM	3	-	8	3	-	-	1	-	-
CRCM_CGCM3	2	1	8	2	-	-	-	-	2
ECP2_GFDL	5	1	3	4	-	-	-	-	2
ECP2_HadCM3	2	1	5	-	-	3	1	1	2
HRM3_HadCM3	2	3	7	2	-	-	1	-	-
MM5I_CCSM	3	-	6	2	-	3	-	-	1
MM5I_HadCM3	4	1	7	1	1	-	1	-	-
RCM3_CGCM3	2	-	9	2	-	-	1	-	1
RCM3_GFDL	2	-	10	2	-	-	1	-	-
WRFG_CCSM	3	1	10	1	-	-	-	-	-
WRFG_CGCM3	2	-	11	1	-	-	1	-	-

On average across future scenarios, snowfall is predicted to decrease by 6.5% and the snowmelt is predicted to decline by 4.4%. As the peak snowfall (Figure 4-2(a)) and snowmelt (Figure 4-2(b)) are predicted to decrease in the future, the proportion of snowmelt contributing to peak flow is projected to decrease. In the other word, the volume of peak flow in the future is more likely to be affected by the future increase in precipitation. Compared with the baseline period, all climate scenarios predicted an increased variability in future peak flow — represented in Fig. 4-1 by a greater distance between opposite ends of the whiskers.

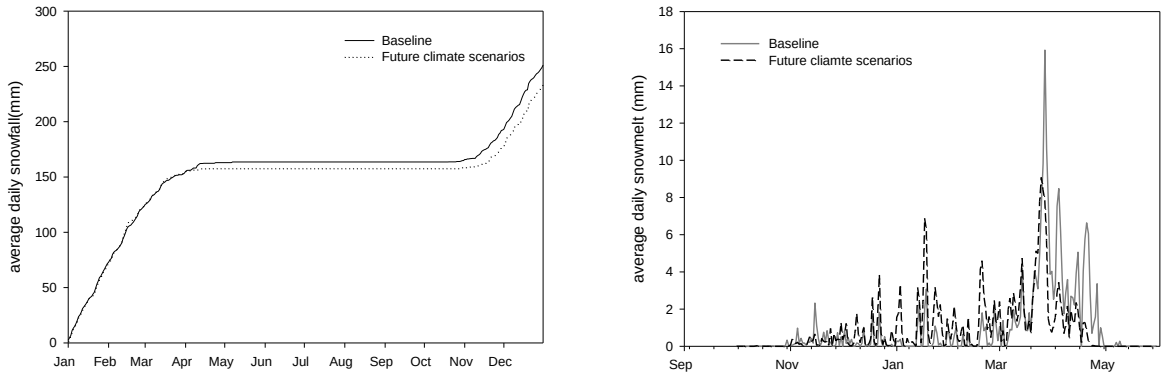

Figure 4-2: Average daily snowfall (a) and snowmelt (b) for future climate scenarios (2053-2067), and for baseline period 1986-2000

4.4.2.3 Separated effects of temperature and precipitation

Using the calibrated ArcSWAT model, the contribution of changed temperature and changed precipitation to peak flow could be assessed by changing the variances of temperature or precipitation independently, i.e. while the variance in temperature was varied, the variance in precipitation was maintained at its level during the baseline period. Accordingly, by modifying the temperature by adding the climate change factor but leaving the precipitation at the same value as during the baseline period, simulated changes in the volume and timing of peak flows could attributed solely to changes in temperature. The individual effects of precipitation and temperature

changes on annual peak flow magnitude (Figure 4-3a and 4-3b, respectively) and on peak flow timing (Tables 4-5 and 4-6, respectively) showed that changing precipitation and leaving temperature unchanged, increased peak flow volume 7% compared over its baseline value, while peak timing remained relatively unchanged. When changing temperature and leaving precipitation unchanged, the volume of peak flow is predicted to decrease by 5% compared with that during the baseline period, and the timing of peak flow occurrences was obviously in advance of that occurring in the baseline period.

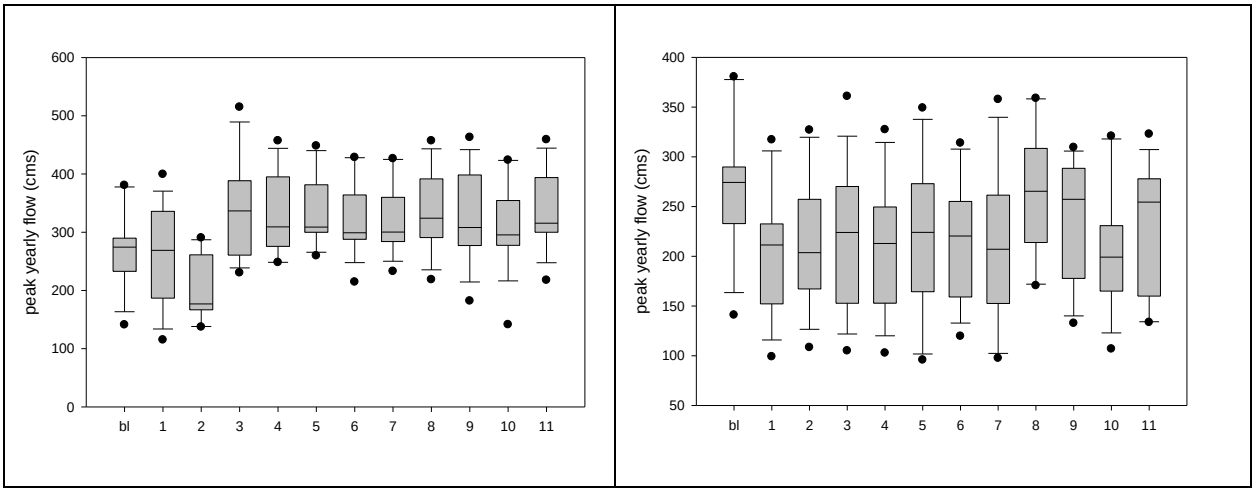

Figure 4-3: Separating effects of precipitation (a) and temperature (b) on peak yearly flow for average future climate scenarios (2053-2067), and for baseline period 1986-2000(Explanation of the x-axis legends: bl: baseline period; 1:CRCM_CCSM; 2:CRCM_CGCM3; 3:ECP2_GFDL; 4:ECP2_HadCM3; 5:HRM3_HadCM3; 6:MM5I_CCSM; 7:MM5I_HadCM3; 8:RCM_CGCM3; 9:RCM3_GFDL; 10:WRFG_CCSM; 11:WRFG_CGCM3)

Table 4-5: Separating effects of precipitation on occurrences of peak flow for each month for all scenarios for 2053-2067, and for baseline period 1986-2000

Climate Scenarios	Jan	Feb	Mar	Apr	May	Jun	Aug	Sep	Nov	Dec
Baseline	2	-	4	6	2	-	-	1	-	-
CRCM_CCSM	1	-	5	7	2	-	-	-	-	-
CRCM_CGCM3	1	-	9	5	-	-	-	-	-	-
ECP2_GFDL	-	-	1	7	7	-	-	-	-	-
ECP2_HadCM3	1	-	2	9	2	-	-	1	-	-
HRM3_HadCM3	1	-	4	7	2	-	-	1	-	-
MM5I_CCSM	1	-	4	2	-	-	-	1	-	-
MM5I_HadCM3	1	-	4	8	2	-	-	-	-	-
RCM3_CGCM3	1	-	4	7	2	-	-	1	-	-

RCM3_GFDL	1	-	3	9	1	-	-	1	-	-
WRFG_CCSM	1	-	4	7	2	1	-	-	-	-
WRFG_CGCM3	1	-	3	8	2	-	-	1	-	-

Table 4-6: Separating effects of temperature on occurrences of peak flow for each month for all scenarios for 2053-2067, and for baseline period 1986-2000

Climate Scenarios	Jan	Feb	Mar	Apr	May	Jun	Aug	Sep	Nov	Dec
Baseline	2	-	4	6	2	-	-	1	-	-
CRCM_CCSM	4	-	8	2	-	-	-	1	-	-
CRCM_CGCM3	3	-	9	2	-	-	-	-	-	1
ECP2_GFDL	4	1	7	2	-	-	-	1	-	-
ECP2_HadCM3	5	1	6	2	-	-	-	-	-	1
HRM3_HadCM3	3	3	6	-	1	-	1	-	-	1
MM5I_CCSM	3	-	9	2	-	-	-	-	-	1
MM5I_HadCM3	6	3	6	-	-	-	-	-	-	-
RCM3_CGCM3	2	-	9	2	-	-	-	1	-	1
RCM3_GFDL	2	-	10	2	-	-	-	1	-	-
WRFG_CCSM	4	1	8	2	-	-	-	-	-	-
WRFG_CGCM3	2	-	10	1	-	-	-	1	-	1

Average snowfall was predicted to significantly increase (28%) with an increase solely in precipitation (Figure 4-4), indicating that more snow would accumulate in the snowpack for a later melt. As a result, over the whole snowmelt season the quantity of snowmelt was forecasted to increase relative to the baseline scenario (Figure 4-5 (a)), though peak snowmelt was predicted to be slightly earlier. On average, with increased temperatures the snowfall was predicted to dramatically decrease (24%) as more precipitation was judged as rainfall (Figure 4-4 (b). The total amount of snowmelt, therefore, decreases significantly because of the reduction of snow accumulation (Figure 4-5 (b)). But the spatial distribution of snowmelt shows that the snowmelt is projected to increase in late winter and early spring, though the peak of snowmelt is projected to decrease by more than 50%. The pattern of snowmelt also suggests, instead of a major peak of snowmelt in the baseline period, there will be more peaks of snowmelt in the future.

The results show that increased precipitation can contribute to an increased peak flow, the reduction of snowfall and a slight decrease in snowmelt. The increased temperature can result in a decreased peak flow, an increased snowfall and a significant rise in snowmelt. When analysing the future peak flows, the combined effects of temperature and precipitation should be considered. The snowfall is projected to decrease by 6% (Figure 4-4(a)). The decreased snowfall caused by increased temperature is the dominant factor affecting the total snowfall in the future, which can offset the increased snowfall caused by increased precipitation. The pattern of snowmelt in the future, as presented in Figure 4-4 (b), is basically consistent with the separated effect of temperature on snowmelt (Figure 4-5(b)). In the future, the increased volume of peak flow can be attributed to the increase of precipitation, while the temporal advance of peak flow occurrence can result from the increased temperature.

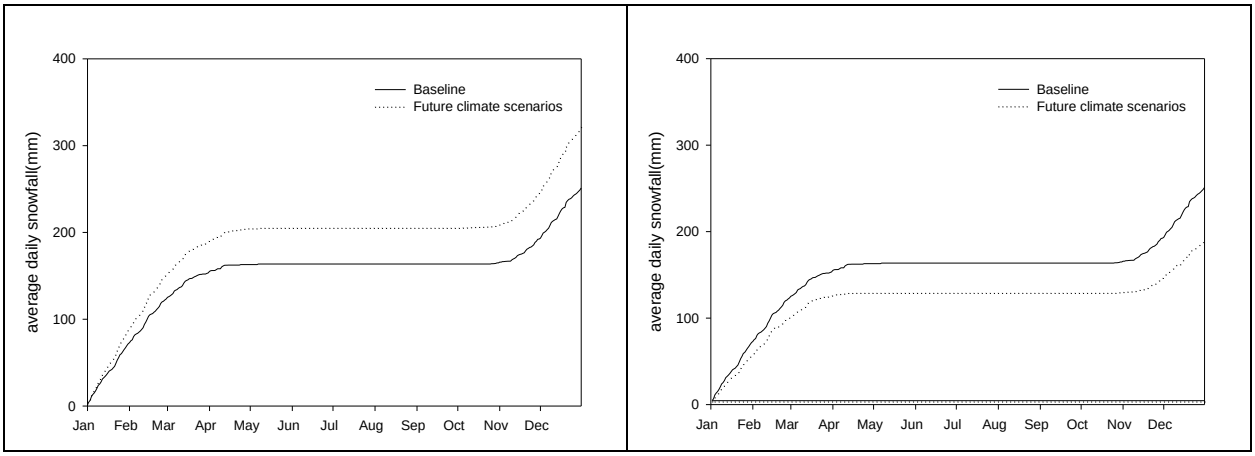

Figure 4-4: Separating effects of precipitation (a) and temperature (b) on average daily snowfall for average future climate scenarios (2053-2067) and for baseline period 1986-2000

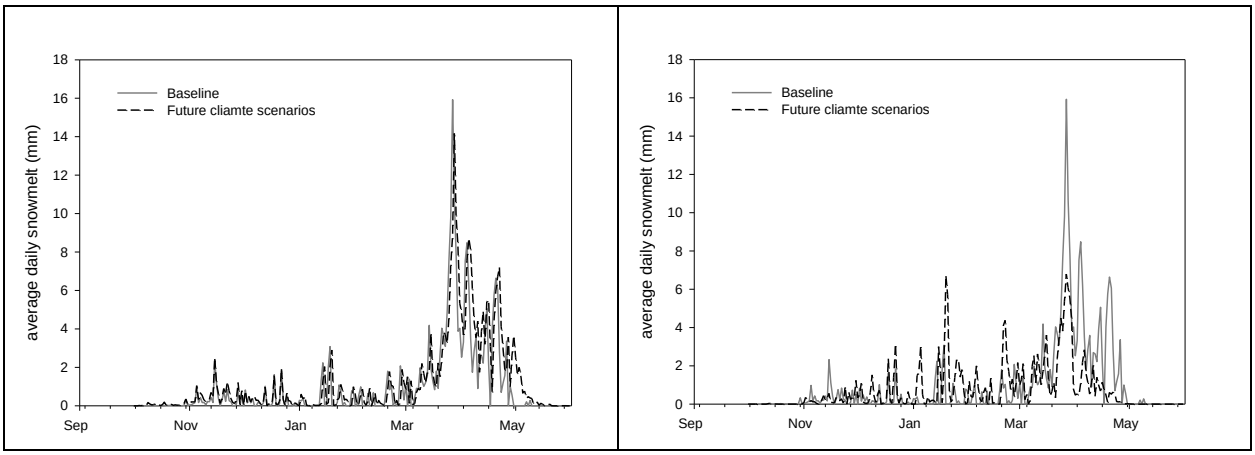

Figure 4-5: Separating effects of precipitation (a) and temperature (b) on average daily snowmelt for average future climate scenarios (2053-2067), and for baseline period 1986-2000

4.5 Discussion and Conclusions

To assess the future hydrologic response of the to climate change, the present study applied future climate projections using a version of the ArcSWAT model calibrated and validated for the watershed in question. The change factor method was introduced to correct the bias between projections and the present baseline situation. An analysis of climatic changes and resulting hydrological changes in the Nicolet River watershed for the future period of 2053-2067, showed all projections suggest an increase in both temperature and precipitation. These changes ranged from 2.0℃ to 3.1℃ and from 12% to 34% for temperature and precipitation, respectively, depending on different climate projections. On average, snowfall is projected to decrease by 6%. The snowmelt is projected to increase in late winter and earlier spring, and the peak of the snowmelt is projected to decrease by approximately 50%. Hydrologic response to climate change can be attributed to combined effects of the temperature and precipitation. The ArcSWAT simulations of future climate scenarios show climate change could result in significant changes in winter streamflow and annual peak flow.

Although the precipitation is projected to increase, the snowfall is predicted to decrease by 6.5% due to the increased temperature. The snowmelt is predicted to decrease by 4.4%. Based on an

analysis of the separate effects of temperature or precipitation on snowmelt, snowmelt was determined to be mainly affected by temperature. On one hand, the reduction of snowfall will reduce the snow stored in the snowpack, thus decreasing the volume of snowmelt. The increased temperature will induce many episodic snow melts and result in an earlier major snowmelt, such that distribution of snowmelt events within a melting season will be altered. The volume of peak flow was predicted to increase by 13% compared to the baseline period, and occurrence of peak flow to be advanced. The study of separating effects of temperature and precipitation on peak flow shows that while the increase in peak flows is dominated by increased precipitation, the timing of peak flow occurrence is mostly affected by the temperature. The contribution of snowmelt to peak flow may diminish, as increased winter temperature induces many episodic snow melts which lead to a reduction of the potential volume of the peak snowmelt. However, the results suggest an increase of spring flood risk, with an average increase of 13% in peak flow, with increased liquid precipitation being responsible for the increase in peak flow. The higher temperature in winter and spring will also lead to earlier snowmelt. The highest frequency of peak flow occurrence for all the scenarios is March, compared with the baseline period which peak flow frequently occurs in April.

Compared to the other studies, the present study focused on discriminating the effects of temperature and precipitation on snowmelt. As the atmospheric CO_2 concentration ($[CO_2]_{atm}$) is an important climate change variable, in future work, the combined effects of changed precipitation and changed temperature, in concert with the different $[CO_2]_{atm}$, on snowmelt should be studied jointly to assess more accurately the potential hydrological responses to climate change. Moreover, the separate effect of $[CO_2]_{atm}$ on snowmelt, peak flow and streamflow should be studied to assess how the different $[CO_2]_{atm}$ values might contribute to high streamflow events.

To conclusion, the annual streamflow witnesses an increase in the future. The increased precipitation could increase the risk of spring flood in the future, while the increased temperature could result in an earlier peak flow.

Chapter 5: Summary and Conclusion

The main objectives of this study were (i) to simulate the streamflow of the Nicolet River Watershed using ArcSWAT model, and (ii) to analyse the impacts of climate change on the hydrology of the study area. The most sensitive parameters for this particular area were identified by sensitivity test, then the model was calibrated and validated against observed streamflow data. The climate change data was provided by the North American Regional Climate Change Assessment Program (NARCCAP). The delta change method was applied to the climate data which generated by embedding the regional climate model (RCMs) into global climate models (GCMs).

Generally, two methods were applied for snowmelt simulating: temperature index method and energy balance method. Most of the models applied the temperature index method to simulate the snowmelt as temperature data is easily accessible.

ArcSWAT model was calibrated and validated for the study area with PBIAS within ±15%, NSE > 0.50, and RSR < 0.70. The sensitive parameters for streamflow were CN2, GW_REVAP, ESCO, SLSOIL, and SOL_AWC. While the CN2 was the most sensitive parameter for surface runoff, ESCO and SLSOIL were the two most sensitive parameters for water yields and subsurface runoff respectively. The model yielded a satisfactory performance in simulating streamflow after calibration with daily NSE of 0.55, RSR of 0.67 and PBIAS of 8.97. The simulated streamflow pattern coincides with the observed streamflow pattern, which indicates two major high flows events in a year: a peak flow in late winter or early spring and a secondary peak flow in summer or autumn. Overall, ArcSWAT provided reasonable streamflow simulations, though the annual flow was slightly underestimated by the model.

ArcSWAT simulations using delta-corrected data suggested that future climate changes could affect the annual and seasonal streamflow, as well as the timing and the amount of peak flow significantly in Nicolet River watershed. All the climate scenarios suggested an increase in average temperature (+2.6 ℃) and precipitation (+21%), and the increases were particularly significant in winter. The mean annual streamflow was projected to increase by 30% in the future. Seasonally, spring streamflow witnessed a decrease of 11 mm, while winter streamflow was projected to increase of 80% compared with the baseline period. For the melting season, on average, the snowfall was projected to decrease by 6.5%, and the snowmelt was forecasted to increase by 4.4%. Thus, the proportion of snowmelt runoff contributing to streamflow was predicted to decrease. Peak flows were predicted to increase by 13% in the future when averaging all the scenarios. The results also showed that the peak flows tended to occur earlier. For the baseline period, most of the peak flows happened in March and April, however, the occurrence time of peak flow moved from April to March under projected climate change.

In this research, the separated effects of temperature and precipitation were firstly studied compared with previous works. This study changes one of these two variances at a time, then keeps another variance same as the value of baseline period. When changing the precipitation and keeping temperature unchanged, with the increasing precipitation, the snowfall was projected to increase 28%. The results showed an increase of 7% for the peak flow against the baseline period, and there was no obvious change in the timing of peak flow occurrence. When changing the temperature and keeping precipitation unchanged, the snowfall was predicted to decrease by 24%. The peak flow was projected to decrease by 5%, and the occurrence of peak flows was observed to advance when comparing with the peak flow occurrence in baseline period. Then pattern of snowmelt changes from a major peak flow to multiple sub-peak flow. To conclude, when

separating the effects of temperature and precipitation on peak flow, the increases in the peak flows are attributed by the increased precipitation, while the timing of the peak flow occurrences is mostly influenced by increased temperature.

References

Andrews, J. (ed). (1993). Flooding: Canada Water Year Book. Ottawa: Ministry of Supply and Services.

Arendt, A., & Sharp, M. (1999). Energy balance measurements on a Canadian high arctic glacier and their implications for mass balance modelling. p. 165-172. In: Interactions Between the Cryosphere, Climate and Greenhouse Gases (Proceedings of IUGG 99 Symposium HS2, Birmingham, July 1999). International Association of Hydrological Sciences Publ. no. 256. Wallingford, UK: IAHS.

Arnold, J., Kiniry, J., Srinivasan, R., Williams, J., Haney, S., and Neitsch, S. (2012a). "Soil and Water Assessment Tool Input/Output Documentation, Version 2012, Texas Water Resources Institute, Temple, TX, USA." TR-439.

Arnold, J. G., Moriasi, D. N., Gassman, P. W., Abbaspour, K. C., White, M. J., Srinivasan, R., Santhi, C., Harmel, R., Van Griensven, A., and Van Liew, M. W. (2012b). SWAT: Model use, calibration, and validation. *Transactions of the ASABE* **55**, 1491-1508.

Arnold, J. G., Srinivasan, R., Muttiah, R. S., and Williams, J. R. (1998). Large area hydrologic modeling and assessment part I: Model development1. Wiley Online Library.

Barnett, T. P., Adam, J. C., and Lettenmaier, D. P. (2005). Potential impacts of a warming climate on water availability in snow-dominated regions. *Nature* **438**, 303-309.

Bergstrom, S. (1976). Development and application of a conceptual runoff model for Scandinavian catchments.

Bøggild, C., Knudby, C., Knudsen, M., and Starzer, W. (1999). Snowmelt and runoff modelling of an Arctic hydrological basin in west Greenland. *Hydrological Processes* **13**, 1989-2002.

Brooks, G., Evans, S., and Clague, J. (2001). Flooding. *A synthesis of natural geological hazards in Canada. Geological Survey of Canada Bulletin* **548**, 101-143.

Caux, P.-Y., Bastien, C., and Crowe, A. (1996). Fate and impact of pesticides applied to potato cultures: the Nicolet River Basin. *Ecotoxicology and environmental safety* **33**, 175-185.

Chen, J., Brissette, F. P., and Leconte, R. (2011). Uncertainty of downscaling method in quantifying the impact of climate change on hydrology. *Journal of Hydrology* **401**, 190-202.

Coulibaly, P., Anctil, F., Rasmussen, P., and Bobee, B. (2000). A recurrent neural networks approach using indices of low‐frequency climatic variability to forecast regional annual runoff. *Hydrological Processes* **14**, 2755-2777.

Ferguson, R. (1999). Snowmelt runoff models. *Progress in Physical Geography* **23**, 205-227.

Ghavidelfar, S., Alvankar, S. R., and Razmkhah, A. (2011). Comparison of the lumped and quasi-distributed Clark runoff models in simulating flood hydrographs on a semi-arid watershed. *Water resources management* **25**, 1775-1790.

Gollamudi, A. (2006). Hydrological and water quality modeling of agricultural fields in Quebec.

Gombault, C., Sottile, M.-F., Ngwa, F. F., Madramootoo, C. A., Michaud, A. R., Beaudin, I., and Chikhaoui, M. (2015). Modelling climate change impacts on the hydrology of an agricultural watershed in southern Québec. *Canadian Water Resources Journal/Revue canadienne des ressources hydriques* **40**, 71-86.

Graham, D., and Klide, L. (2002). MIKE SHE User Guide. *Danish Hydraulic Institute, Denmark.*

Hock, R. (2003). Temperature index melt modelling in mountain areas. *Journal of hydrology* **282**, 104-115.
Huntington, S. P. (2006). "Political order in changing societies," Yale University Press.
IPCC (2013). "Climate Change 2013: The Physical Science Basis. Contribution of Working Group I to the Fifth Assessment Report of the Intergovernmental Panel on Climate Change," Cambridge University Press, Cambridge, United Kingdom and New York, NY, USA.
Lemonds, P. J., and McCray, J. E. (2007). Modeling hydrology in a small rocky mountain watershed serving large urban populations. *JAWRA Journal of the American Water Resources Association* **43**, 875-887.
Maréchal, D. (2004). A soil-based approach to rainfall-runoff modelling in ungauged catchments for England and Wales.
Martinec, J., and Rango, A. (1986). Parameter values for snowmelt runoff modelling. *Journal of Hydrology* **84**, 197-219.
Mazouz, R., Assani, A. A., Quessy, J.-F., and Légaré, G. (2012). Comparison of the interannual variability of spring heavy floods characteristics of tributaries of the St. Lawrence River in Quebec (Canada). *Advances in Water Resources* **35**, 110-120.
Minville, M., Brissette, F., and Leconte, R. (2008). Uncertainty of the impact of climate change on the hydrology of a nordic watershed. *Journal of hydrology* **358**, 70-83.
Moriasi, D. N., Arnold, J. G., Van Liew, M. W., Bingner, R. L., Harmel, R. D., and Veith, T. L. (2007). Model evaluation guidelines for systematic quantification of accuracy in watershed simulations. *Trans. Asabe* **50**, 885-900.
Mortsch, L., Lister, M., Lofgren, B., Quinn, F., and Wenger, L. (1999). Climate change impacts on hydrology, water resources management and the people of the Great Lakes–St. *Lawrence System: A Technical Survey, A Report for the IJC Reference on Consumption, Diversions and Removals of Great Lakes Water, Environment Canada, Toronto*.
Nash, J. E., and Sutcliffe, J. V. (1970). River flow forecasting through conceptual models part I—A discussion of principles. *Journal of hydrology* **10**, 282-290.
Neitsch, S. L., Arnold, J. G., Kiniry, J. R., and Williams, J. R. (2011). "Soil and water assessment tool theoretical documentation version 2009." Texas Water Resources Institute.
Noor, H., Vafakhah, M., Taheriyoun, M., and Moghadasi, M. (2014). Hydrology modelling in Taleghan mountainous watershed using SWAT. *Journal of Water and Land Development* **20**, 11-18.
Organization, W. M. (1986). "Intercomparison of models of snowmelt runoff," World Meteorological Organization.
Quémerais, B., Lemieux, C., and Lum, K. R. (1994). Temporal variation of PCB concentrations in the St. Lawrence river (Canada) and four of its tributaries. *Chemosphere* **28**, 947-959.
Rango, A., and Martinec, J. (1995). Revisiting the degree-day method for snowmelt computations. *JAWRA Journal of the American Water Resources Association* **31**, 657-669.
Ritchie, J. T. (1972). Model for predicting evaporation from a row crop with incomplete cover. *Water resources research* **8**, 1204-1213.
Seibert, J. (2005). HBV light version 2, user's manual. *Stockholm University-available at* http://people. *su. se/~ jseib/HBV/HBV_manual_2005. pdf.*

Shrestha, R. R., Dibike, Y. B., and Prowse, T. D. (2012). Modelling of climate-induced hydrologic changes in the Lake Winnipeg watershed. *Journal of Great Lakes Research* **38**, 83-94.

Singh, J., Knapp, H. V., Arnold, J., and Demissie, M. (2005). Hydrological modeling of the iroquois river watershed using HSPF and SWAT1. Wiley Online Library.

Stewart, I. T. (2009). Changes in snowpack and snowmelt runoff for key mountain regions. *Hydrological Processes* **23**, 78-94.

Tarboton, D. G., and Luce, C. H. (1996). "Utah energy balance snow accumulation and melt model (UEB)," Utah Water Research Laboratory.

Troin, M., and Caya, D. (2014). Evaluating the SWAT's snow hydrology over a Northern Quebec watershed. *Hydrological Processes* **28**, 1858-1873.

Wang, X., and Melesse, A. (2005). Evaluation of the SWAT model's snowmelt hydrology in a northwestern Minnesota watershed. *Transactions of the ASAE* **48**, 1359-1376.

Ward, R. (1989). Hydrology of floods in Canada: a guide to planning and design. *National Research Council Canada, Ottawa* **245**.

Whitfield, P. H., and Cannon, A. J. (2000). Recent variations in climate and hydrology in Canada. *Canadian Water Resources Journal* **25**, 19-65.

Wu, K., and Johnston, C. A. (2007). Hydrologic response to climatic variability in a Great Lakes Watershed: A case study with the SWAT model. *Journal of Hydrology* **337**, 187-199.

Yagouti, A., Boulet, G., Vincent, L., Vescovi, L., and Mekis, E. (2008). Observed changes in daily temperature and precipitation indices for southern Québec, 1960–2005. *Atmosphere-Ocean* **46**, 243-256.

Zhang, X., Vincent, L. A., Hogg, W., and Niitsoo, A. (2000). Temperature and precipitation trends in Canada during the 20th century. *Atmosphere-ocean* **38**, 395-429.